(Pricop et al., 1993). Higher concentrations (>100-fold) were required for binding of IgM monomers to the FcμR+ cells than IgM pentamers, indicating the importance of IgM ligand configuration (Fig. 2 C). Collectively, these results indicate that the previously identified FAIM3/TOSO is an authentic FcμR with exclusive and high affinity binding specificity for the Fc portion of IgM.

The Ig domain of FcμR is similar but distantly related to that of pIgR and Fcα/μR

FCMR is a single copy gene located on chromosome 1q32.2, adjacent to two other IgM-binding receptor genes, *PIGR* and *FCAMR*. The Ig-like domain of FAIM3/TOSO/FcμR is thought to be involved in the binding of agonistic IgM anti-Fas mAb (Hitoshi et al., 1998). A comparison of the protein sequence of the Ig-binding domains of FcμR, pIgR, and Fcα/μR to the pIgR structural data reported by Hamburger et al. (2004) provided some potential insight into ligand specificity (Fig. 3). In addition to a disulfide bond between Cys22 and Cys92 linking the two β sheets (B and F strands), a second disulfide bond between Cys38 and Cys46 linking the C and C′ strands is also conserved in all three receptors. Arg63 and Asp86 are also completely conserved, but Trp37 is found only in the pIgR and Fcα/μR. Several other residues (Gly6, Tyr24, Val29, Arg31, Lys35, Tyr55, and Leu101) are also conserved in pIgR and Fcα/μR but not in FcμR. A major difference between FcμR and the other two receptors is in the CDR1 region. The CDR1 of the pIgR from six different species consists of 9 aa (Pro25 to Thr33), and this is also the case in the Fcα/μR from two different species. In contrast, the corresponding region of the FcμR from seven different species consists of 5 aa and has a noncharged residue (Met, Leu, or Thr) at the position corresponding to Arg31, which has been shown to be solvent exposed and possibly to interact directly with polymeric IgA in the human pIgR (Hamburger et al., 2004). These results suggest a structural basis for the distinct mode of IgM interactions with FcμR versus pIgR and Fcα/μR.

Conserved Ser and Tyr residues in the cytoplasmic tail of FcμR

A charged His residue is adjacent to or within the putative 19-aa transmembrane segment of FcμR from all species examined except for the bovine (Fig. 4). The 118-aa cytoplasmic

```
                    10        20        30        40          50        60
            ....|....|....|....|....|....|....|....|. ...|....|....|....|....|....
hu pIgR     KSPIFGPEEVNSVEGNSVSITCYYPPTSVNRHTRKYWCRQG-ARGGCITLISSEGYVSSKYAGRANLTNF
rb pIgR     P.S....G...VL..D.........T...T..S..F...EE-ES.R.V..A.T-..T.QE.S..GK..D.
mo pIgR     .......Q..S.I..D.........D..............-.S.M.T....N..L.KE.S.....I..
rt pIgR     Q......QD.S.I............D..............-.N.Y.A....N..L.KE.S...S.I..
bo pIgR     ...........T....R....K..................-.Q.R.T.........DD.V.......
ch pIgR     LN.V....QQ.YGLIDG....K.F....T....D......ES-S.S-.L.VV.TS..RARG.Q..VTIID.
hu Fcα/μR   PNSLK.SRL.SGEP.GA.T.Q.H.A.S.....Q.......L.PP.WI.Q.IV.TNQ.THHR.RD.VA..D.
mo Fcα/μR   TNALR..RL.TGNT.GA.T.H.H.A.S.....Q.......L.SPLWI.H.VV.TNQ.THPD.R...A..DI
hu FcμR     --R.LPEVK.EGEL.G..T.K.PL.----EM.V.I.L..EMAGS.T.G.VV.TTNFIKAE.K..VT.KQY
cm FcμR     --R.LPEVK.EGEL.G..T.K.PL.----EM.V.I.L..EMAGS.T.G.VV.TTNFIKAE.K..VT.KQY
mn FcμR     --R.LPEVK.EGEL.G..T.K.PL.----EM.V.M.L..EMVES.T.G.VV.TTNFIKVE.KH.VT.KQY
bo FcμR     --KVLPEVKMEGML.G.IT.E.PL.----ET.V.I.L..TIDES.R.T.VV..NK..REEFKH.VT.EQC
do FcμR     --R.LPEVKMEGEL.G.IT.E.PL.----QM.V.L.L..EIAES.V.A.VV.NKNF.KEE.KH.VT.KPC
mo FcμR     --RVLPEVQL.VEW.G.II.E.PL.----QL.V.M.L...MAKP.I.S.VV.NT-F.KKE.ER.VT..PC
rt FcμR     --KVLPEVRLEVEL.G..F.E.PL.----QT.V.M.L...MTNPAI.A.VV.NI-F.KKE.KR.VT.KPS
            70        80        90        100       110
            |....|....|....|....|....|.... |....|....|.
hu pIgR     PENGTFVVNIAQLSQDDSGRYKCGLGINSR-GLSFDVSLEV--
rb pIgR     .DK.E...TVD..T.N...S....V.V.G.-..D.G.NVL.--
mo pIgR     ...N...I..E..T...T.S.......TSN.-...........--
rt pIgR     ...S...I...H.T.E.T.S.......TTN.-..F.......--
bo pIgR     ..S.....D.SH.THK............S..-..N.......--
ch pIgR     ..Q.IML...S..TLA.Q.T.Q..I.L.GK-...NR...DI--
hu Fcα/μR   .QR.L...RLS...P..I.C.L..I.SENN-M.FLSMN.TI--
mo Fcα/μR   .QS.L...RLLR..LG.V.L.R..I.DRND-M.F.S.N.T.--
hu FcμR     .RKNL.L.EVT..TES...V.A..A.M.TDR.KTQK.T.N.HS
cm FcμR     .HKNL.L.EVT..TES...V.A..A.M.TDR.KTQK.T.N.HS
mn FcμR     .RKNL.L.EVT..TES...V.A..A.R.TDR.KTQK.T.N.HS
bo FcμR     .DRNL.L.VMTE.TKN...I.A..V.G.TDR.KTQQIT.T.HS
do FcμR     .DRKL.L.EVTE.TKS...I.A..T.M.TDR.KTQQ.T.S.HS
mo FcμR     LDKKL.L.EMT..TEN.D.I.A..V.MKTDK.KTQKIT.N.HN
rt FcμR     LNKKL.L.EMT..TK..E.I.A..V.T.TDL.KTQK.T.N.RN
```

Figure 3. aa sequence alignment of IgM-binding receptors. The Ig-binding domains of pIgR, Fcα/μR, and FcμR from several species were aligned using the CLUSTAL W multiple alignment program (Thompson et al., 1994). aa identity is indicated by dots and gaps are indicated by dashes. Residues conserved in all three receptors and in pIgR and Fcα/μR are highlighted in yellow and red, respectively. The numbers indicate the aa position from the N terminus of the Ig-binding domain of human pIgR. These sequences are available from GenBank/EMBL/DDBJ under the following accession nos.: pIgR of human (hu; P01833), rabbit (rb; P01832), mouse (mo; O70570), rat (rt; P15083), bovine (bo; P81265), and chicken (ch; AAP69798); Fcα/μR of human (AAL51154) and mouse (NP_659209); and FcμR of human (NP_005440), chimpanzee (cm; XP_001165341), monkey (mn; XP_001084243), bovine (XP_588921), dog (do; XP_547385), mouse (NP_081252), and rat (Q5M871).

tail is composed of a basic aa-rich region, a Pro-rich region, two conserved Cys residues, and an acidic aa-rich region in all seven different FcμRs. Of the Ser residues, five are completely conserved and an additional four are highly conserved among these FcμRs, and some of them are potential sites for protein kinase C (PKC) phosphorylation (R/$K_{1\text{-}3}$-$X_{0\text{-}2}$-S/T-$X_{0\text{-}2}$-R/$K_{1\text{-}3}$ or R/K-X-S-Z-R/K, where Z represents a hydrophobic aa residue) or casein kinase 2 phosphorylation (S/T-X_2-D/E). Three Tyr residues are also completely conserved among these FcμRs, but none of them (I/V-Y315-S/T-A-C, S-C-E/D-Y361-V-S, and S-D-D-Y385-I/V-N-V/I) match the immunoreceptor tyrosine-based activation motif (D/E-X_2-Y-X_2-L/I-$X_{6\text{-}8}$-Y-X_2-L/I), inhibitory motif (I/V-X-Y-X_2-L/V), or switch motif (T-X-Y-X_2-V/I). However, if phosphorylated, the most carboxyl tyrosine is a potential binding site (pY-X-N-X) for the Src homology 2 domains of growth factor receptor–bound protein 2 and growth factor receptor–bound protein 2–related adaptor protein, as observed in transmembrane adaptor proteins, including linker for activation of T cells and non–T cell activation linker (Horejsí et al., 2004). These findings indicate a quite distinct feature of the FcμR cytoplasmic tail compared with other FcRs, in which the Ig ligand binding chains are usually devoid of conserved Tyr residues except for FcγRIIA and FcγRIIB.

To determine whether these conserved Ser and Tyr residues are phosphorylated upon stimulation, FcμR⁺ BW5147 T cells were treated with a tyrosine phosphatase inhibitor, pervanadate, or with preformed IgM immune complexes to cross-link FcμR. The FcμR was immunoprecipitated from the lysates of resting or activated cells and analyzed by immunoblotting with antibodies specific for phosphotyrosine or the phosphoserine of PKC substrates. Phosphorylation of both serine and tyrosine residues was clearly demonstrated in pervanadate-treated cells but not in untreated cells (Fig. 5 A). Interestingly, the serine-phosphorylated FcμR migrated at ~52 kD, whereas most of the tyrosine-phosphorylated FcμRs migrated at ~60 kD and, to a lesser extent, at ~52 kD. When these membranes were reprobed with anti-FcμR mAb specific for its extracellular epitope, we found that in resting cells FcμR was present as a major band of ~60 kD, which is consistent with the M_r of the cell-surface FcμR (see Fig. 7), along with a minor band of ~45 kD, but in pervanadate-treated cells the FcμR was resolved as a major band of ~52 kD together with multiple minor species of various sizes. When FcμR was cross-linked with preformed immune complexes consisting of IgM and F(ab')$_2$ fragments of anti-μ mAb, phosphorylation of both serine and tyrosine residues of the ~52 kD FcμR was also demonstrated as early as 3 min after ligation. The serine phosphorylation became more prominent at 30 min after ligation, whereas tyrosine phosphorylation was diminished by that time point (Fig. 5 B). In contrast to the effects seen with pervanadate treatment, tyrosine-phosphorylated ~60-kD FcμR was not observed in the lysates of receptor-ligated cells. Reprobing of these membranes with anti-FcμR mAb revealed the presence of both ~60- and ~52-kD FcμR proteins as well as minor, but discrete, bands of ~45 and ~63 kD. Collectively, these findings suggest that the conserved serine and tyrosine residues seen in the cytoplasmic tail of FcμR are indeed potentially phosphorylated upon receptor ligation and that the phosphorylated FcμR protein migrates differently on SDS-PAGE compared with its unphosphorylated form.

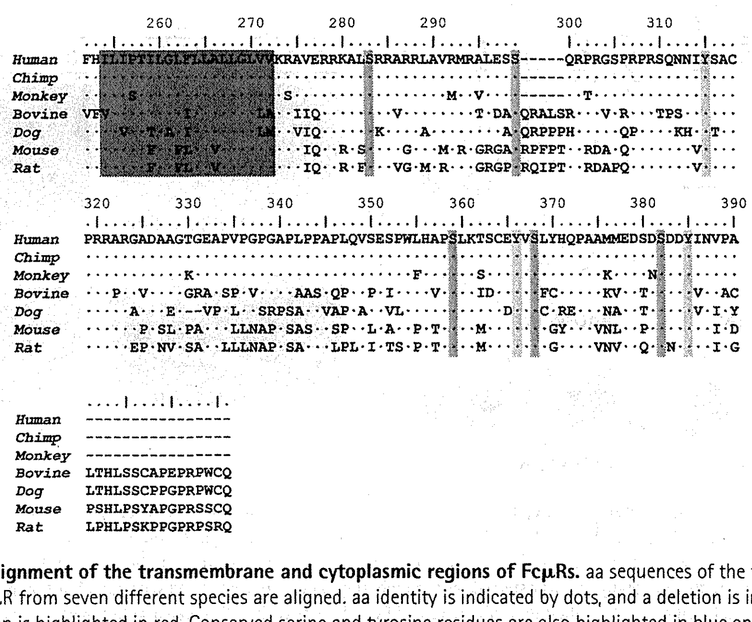

Figure 4. aa sequence alignment of the transmembrane and cytoplasmic regions of FcμRs. aa sequences of the transmembrane segments and cytoplasmic tails of FcμR from seven different species are aligned. aa identity is indicated by dots, and a deletion is indicated by dashes. The predicted transmembrane region is highlighted in red. Conserved serine and tyrosine residues are also highlighted in blue and yellow, respectively. The numbers indicate the aa position from the first Met residue of human FcμR. The GenBank/EMBL/DDBJ accession nos. for these FcμRs are the same as those in Fig. 3. Chimp, chimpanzee.

FcμR per se has no antiapoptotic activity

To determine whether FcμR inhibits Fas-mediated apoptosis as originally described for FAIM3/TOSO (Hitoshi et al., 1998), retroviral constructs containing both FcμR and GFP cDNAs or only the GFP cDNA were transduced into the apoptosis-prone Jurkat human T cell line. Cells expressing comparable levels of GFP were enriched from each transductant by FACS, and the FcμR/GFP transductant was found to express relatively high levels of cell-surface FcμR as determined by both receptor-specific mAbs (see next section) and IgM ligand binding (Fig. 6 A). The resultant FcμR$^+$GFP$^+$ or GFP$^+$ Jurkat cells and nontransduced Jurkat cells as an additional control were then subjected to apoptosis assays using agonistic anti-Fas mAbs of the IgM or IgG$_3$ isotype. Cross-linkage of Fas with the IgM antibody induced robust early (annexin V$^+$/7-aminoactinomycin D [7-AAD]$^-$) and late (annexin V$^+$/7-AAD$^+$) apoptotic cells as well as dead cells (annexin V$^-$/7-AAD$^+$) in the nontransduced Jurkat cells and the GFP$^+$ cells, but not in the FcμR$^+$/GFP$^+$ cells (Fig. 6 B). This result is consistent with the previously reported antiapoptotic activity of FAIM3/TOSO (Hitoshi et al., 1998). It should be noted, however, that addition of control IgM of either human or mouse origin at a 100-fold molar excess into these cultures did not make the FcμR$^+$/GFP$^+$ cells susceptible to IgM anti-Fas mAb-induced apoptosis, suggesting that the simultaneous dual binding to Fas and FcμR (i.e., cis interaction) is dominant over the single binding to FcμR (i.e., trans interaction) in this apoptosis model (Fig. S4). Unlike the effect seen with IgM anti-Fas mAb, ligation of Fas receptor with the IgG$_3$ antibody induced apoptosis in all three cell types, including the FcμR$^+$GFP$^+$ cells. Notably, ligation of FcμR and Fas with the corresponding mAbs either in the absence (i.e., separate ligation of each receptor) or presence of a common secondary reagent (i.e., coligation of both receptors) had no demonstrable effects on the IgG$_3$ anti-Fas mAb–induced apoptosis of FcμR$^+$GFP$^+$ cells. Essentially identical results using IgM versus IgG$_3$ anti-Fas mAb were also obtained with EBV-transformed B cell lines expressing both endogenous FcμR and Fas on their cell surface (unpublished data). Collectively, these findings indicate that FcμR has no intrinsic activity to inhibit Fas-mediated apoptosis, but they raise the interesting possibility that IgM anti-Fas autoantibody, if present in individuals with autoimmune disorders, could interrupt Fas-mediated signaling via FcμR in vivo.

To determine if FcμR could also affect apoptosis mediated through the BCR, the same retroviral constructs as used for Jurkat cells were transduced into a mouse immature B cell line, WEHI231, and a human germinal center B cell line, Ramos, both of which are negative for FcμR expression and are known to undergo apoptosis after BCR cross-linking. However, unlike the Jurkat T cell line, no cell lines of either type that stably expressed both FcμR and GFP were obtained after multiple attempts in different laboratories (unpublished data), whereas control GFP$^+$ cell lines were easily established. Even after enriching GFP^{hi} cells by FACS or by antibiotic selection, the established cell lines were found to express low levels of GFP and no cell-surface expression of FcμR. Flow cytometric analysis of these B cell lines shortly

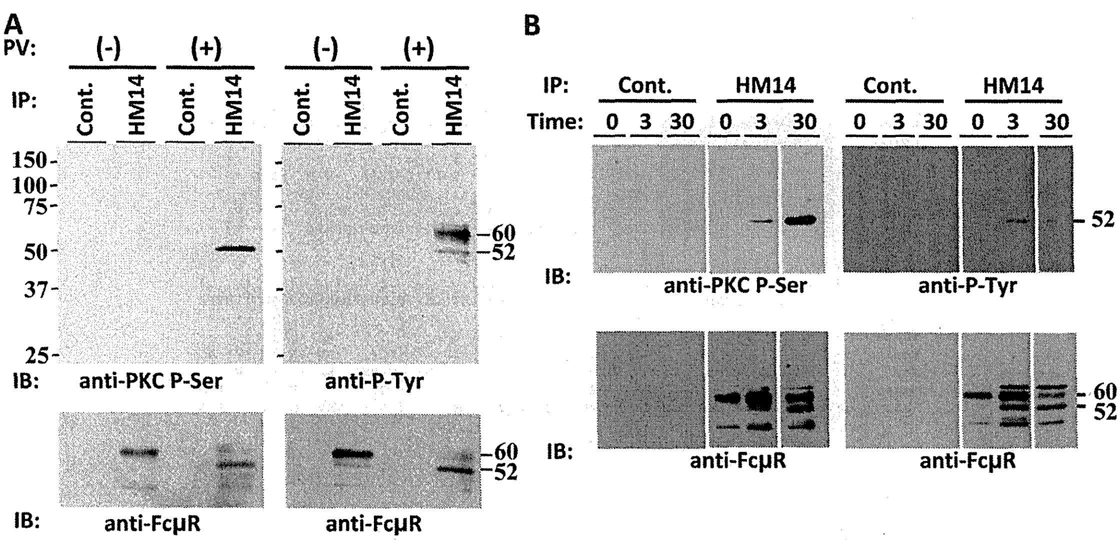

Figure 5. Tyrosine and serine phosphorylation of FcμR upon stimulation. (A and B) BW5147 T cells stably expressing human FcμR were incubated in the presence (+) or absence (−) of 100 μM pervanadate for 15 min (A) or with the preformed IgM immune complexes for the indicated time periods (min) at 37°C (B) before cell lysis. FcμR was immunoprecipitated from cleared lysates with anti-FcμR (HM14) or control (Cont.) mAb-coupled beads, resolved on SDS–10% PAGE under reducing conditions, transferred onto membranes, and immunoblotted with rabbit antibody specific for phosphoserine of PKC substrates along with HRP-labeled goat anti-rabbit Ig antibody (anti-PKC P-Ser) or with HRP-labeled antiphosphotyrosine mAb (anti–P-Tyr) before visualization by ECL. After dissociating blotted antibodies, membranes were reprobed with biotin-labeled anti-FcμR mAbs along with HRP-labeled SA (anti-FcμR). These experiments were performed at least three times. M_r is shown in kilodaltons.

after transduction revealed that forced expression of FcμR resulted in down-modulation of their cell-surface IgM, presumably because of its ligation with the FcμR, thereby leading to loss of the FcμR$^+$GFP$^+$ cell population. Thus, these findings suggest that the ectopic expression of FcμR on WEHI231 and Ramos B cell lines triggers BCR-mediated apoptosis as a consequence of direct interaction between the FcμR and membrane-bound IgM molecules.

FcμR is an ~60-kD transmembrane protein

Two hybridoma mAbs specific for human FcμR, HM7 (γ2bκ), and HM14 (γ1κ) were established from mice immunized with FcμR$^+$ BW5147 T cells and were used along with the IgM ligand for biochemical characterization of the receptor. The HM7 mAb appeared to recognize an epitope near the IgM ligand binding site, because HM7 antibody binding was significantly inhibited by preincubation of FcμR$^+$ cells with IgM, whereas HM14 binding was not (unpublished data). Our earlier biochemical analysis revealed that FcμR on B-lineage cells could be attached to the plasma membrane via a glycosylphosphatidylinositol (GPI) linkage (Ohno et al., 1990; Nakamura et al., 1993), but the structure predicted by the cDNA is of a transmembrane protein. We thus reexamined this issue using a highly purified GPI-specific phospholipase C (GPI-PLC). After GPI-PLC treatment, the surface expression of the GPI-anchored Thy-1 on FcμR$^+$ BW5147 T cells was reduced by ~65%, whereas surface FcμR levels were unaffected as determined by staining with both anti-FcμR mAbs and the IgM ligand (Fig. 7 A). As expected, levels of the control transmembrane glycoprotein CD11a were also unaffected. We extended this analysis to the 697 pre–B cell line. Consistent with our previous IgM-binding results (Ohno et al., 1990), these cells do not constitutively express cell-surface FcμR, but its expression could be induced by PMA treatment (Fig. S5). After GPI-PLC treatment, the surface levels of FcμR and CD19 on PMA-activated 697 pre–B cells were unchanged, whereas the expression of GPI-anchored CD73 was reduced by ~50% (Fig. 7 B). Thus, these findings indicate that FcμR is an authentic transmembrane protein, consistent with the predicted structure encoded by the FcμR cDNA.

To determine the M_r of FcμR, we performed SDS-PAGE analysis of biotinylated cell-surface proteins that were precipitated from membrane lysates with anti-FcμR mAbs and IgM ligands. A major protein with an M_r of ~60 kD was precipitated from the FcμR-bearing but not control BW5147 T cells with both probes (Fig. 7 C). The same M_r estimate was obtained under both reducing and nonreducing conditions, indicating that there are no interchain disulfide linkages of FcμR with itself or other proteins. Removal of sialic acid residues with neuraminidase from the ~60-kD FcμR resulted in a decrease in M_r to ~50 kD. The cell-surface FcμR isolated from PMA-activated 697 pre–B cells and normal adult blood mononuclear cells (MNCs) had an identical M_r of ~60 kD, consistent with our previous size estimates (Sanders et al., 1987; Ohno et al., 1990; Nakamura et al., 1993). An additional minor band of ~40 kD was occasionally identified in the precipitates from membrane lysates of FcμR$^+$ BW5147 T cells with anti-FcμR mAbs irrespective of detergents used (NP-40, digitonin, or CHAPS). The molecular identity of this 40-kD

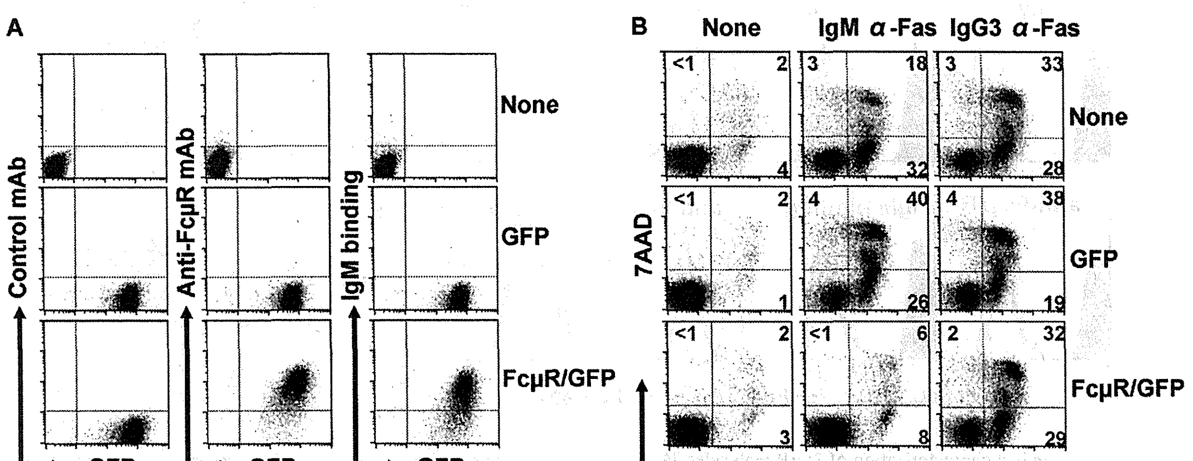

Figure 6. Role of FcμR in Fas-mediated apoptosis of Jurkat T cells. (A) Jurkat cells transduced without (none) or with the bicistronic retroviral construct containing GFP cDNA only (GFP) or both FcμR and GFP cDNAs (FcμR/GFP) were incubated with biotin-labeled isotype-matched control mAb (left), HM14 anti-FcμR mAb (middle), or human IgM (right), and then with APC-SA before analysis by FACSCalibur. Note the comparable levels of GFP in both GFP and FcμR/GFP transductants, and the expression of FcμR on the FcμR/GFP transductant as determined by anti-FcμR reactivity and IgM ligand binding. (B) These three cell lines were incubated at 37°C for 24 h with agonistic anti-human Fas mAbs of mouse IgMκ (CH11 clone; 10 ng/ml) or $IgG_3κ$ isotype (2R2 clone; 0.3 μg/ml). Cells were stained with 7-AAD and APC-labeled annexin V before identification of early (annexin V$^+$/7-AAD$^-$) and late (annexin V$^+$/7-AAD$^+$) apoptotic and dead (annexin V$^-$/7-AAD$^+$) cells by FACSCalibur. Note the resistance of FcμR/GFP transductant to IgM but not IgG3 anti-Fas mAb-induced apoptosis. Numbers indicate percentages of cells. These experiments were performed more than three times.

protein is presently unknown. Although the predicted pI of FcμR is ~9.9, the ~60-kD FcμR was resolved into a spot with a pI of ~5 by two-dimensional gel electrophoresis analysis (unpublished data), consistent with our previous finding that FcμR is sialylated (Ohno et al., 1990).

FcμR is predominantly expressed by both B and T lymphocytes

To determine the cellular distribution of FcμR, we first conducted RT-PCR analysis of various tissues and a panel of representative cell lines. FcμR transcripts were restricted to hematopoietic and lymphoid tissues, including the blood, bone marrow, tonsils, spleen, and appendix. FcμR transcripts were detected in both $CD4^+$ and $CD8^+$ T cells from blood as well as in all subsets of tonsillar B cells, although the transcript levels appeared highest in the follicular and memory B cells (Fig. S6, top). Among the cell lines, 697 pre–B cells expressed FcμR transcripts, although they did not constitutively express cell-surface FcμR protein (Fig. S5). Another pro-/pre-B cell line (REH) and some B cell lines (Ramos and the EVB-transformed line BDB-14.4) also contained FcμR mRNA (Fig. S6, bottom).

Next, we examined cell-surface FcμR expression by immunofluorescence analysis using receptor-specific mAbs and IgM ligands. In normal adult blood samples, FcμR was clearly expressed on $CD19^+$ B cells and on the $CD4^+$ and $CD8^+$ T cells, although there was no discrete demarcation between $FcμR^+$ and $FcμR^-$ T cells (Fig. 8 A). The intensity of staining with the HM14 mAb was higher than with the HM7 mAb (unpublished data), an observation consistent with the finding that the HM7 epitope is sensitive to IgM ligand binding; given its high affinity, the FcμR is likely to be occupied by IgM in vivo. Clearly, mAb reactivity was a more sensitive assay for the detection of FcμR than ligand binding using biotin-labeled human IgM, although the sensitivity of the ligand-binding assay could be increased by using mouse IgMκ, biotin-labeled rat anti–mouse κ mAb and streptavidin (SA)-PE. In addition to B and T cells, $CD56^+/CD3^-$ NK cells also expressed FcμR at relatively low density. Other blood cell types, $CD14^+$ monocytes, $CD13^+$ granulocytes, erythrocytes, and platelets, did not express FcμR at detectable levels (Fig. S7).

Notably, overnight culture of blood MNCs in IgM-free media enhanced FcμR expression especially by T cells (Fig. 8 B), consistent with our previous IgM-binding data (Nakamura et al., 1993). Curiously, this enhancement was more evident for the cell preparations from the tonsils and spleen than from blood. Freshly isolated tonsillar MNCs, including B and T cells, had no reactivity with either anti-FcμR mAbs or IgM ligands, but after overnight culture, there was clear-cut expression of FcμR on the surface of the $CD19^+$ B cells and the $CD4^+$ and $CD8^+$ T cells (Fig. 8 C). Most follicular ($IgD^+/CD38^-$) and memory ($IgD^-/CD38^-$) B cells expressed FcμR, whereas only a small subpopulation of the germinal center ($IgD^-/CD38^+$) and pregerminal center ($IgD^+/CD38^+$) B cells expressed FcμR, consistent with our RT-PCR data. Many

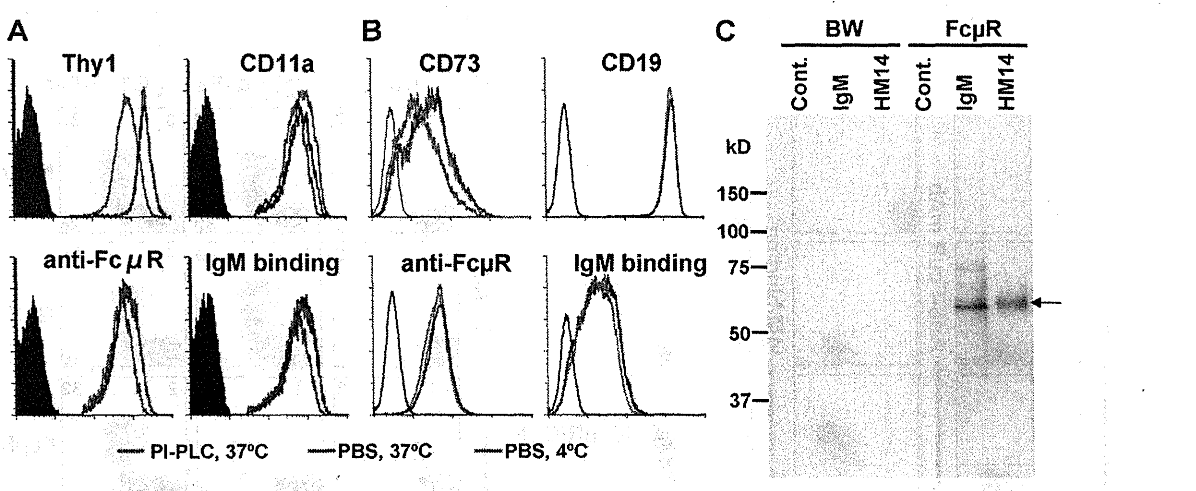

Figure 7. Biochemical characterization of FcμR molecules. (A and B) GPI-PLC treatments. BW5147 T cells stably expressing human FcμR (A) and PMA-activated 697 pre–B cells (B) were incubated with PBS (blue) or 10 U/ml GPI-PLC (red) for 30 min at 30°C, and then examined for the expression of FcμR by anti-FcμR mAb or IgM ligand binding along with the expression of Thy-1 and CD11a (A) or of CD73 (ecto-5′-nucleotidase) and CD19 (B). A control sample was kept on ice during this treatment without GPI-PLC (green). Note the significant reduction in MFI of Thy-1 and CD73 but not of CD11a, CD19, FcμR, and IgM-binding profiles after GPI-PLC treatment. (C) SDS-PAGE analysis of cell-surface proteins. Plasma membrane proteins on control (BW) and FcμR-bearing BW5147 T cells (FcμR) were labeled with biotin, quenched, and incubated with mouse γ1κ control (Cont.) or anti-FcμR (HM14) mAbs or mouse IgMκ ligand before washing and solubilization in 1% NP-40 lysis buffer containing protease inhibitors. The mAb-bound cell-surface proteins were captured by addition of beads coupled with rat anti–mouse κ mAb (187.1 clone) and resolved on SDS–10% PAGE under nonreducing (not depicted) and reducing conditions, followed by transfer onto membranes, blotting with HRP-SA, and visualization by ECL. The same results were obtained with the HM7 anti-FcμR mAbs. The arrow indicates FcμR. The experiments were performed 3 times for A and B and >10 times for C.

CD4+ T cells and the majority of CD8+ T cells clearly expressed cell-surface FcμR after culture. After overnight culture, the proportion of FcμR+ B, CD4+ T, CD8+ T, and NK cells in the spleen was similar to that in blood samples (unpublished data). In adult bone marrow, a small subpopulation (~21%) of the CD19+/surface IgM− pro–/pre–B cells expressed low levels of FcμR on their cell surface, whereas ~42% of the CD19+/surface IgM+ B cells expressed slightly higher levels of FcμR, indicating that FcμR expression begins at the pro–/pre–B cell stage in B-lineage differentiation (Fig. 8 D). No FcμR expression was observed on myeloid cells even after overnight culture in IgM-free media. In contrast to the FcμR phenotype of humans, our initial immunofluorescence analysis of mouse splenocytes with a receptor-specific mAb revealed that FcμR was expressed by B220+ B cells but not by CD3+ T cells or Mac-1+ macrophages (unpublished data).

To further examine the effects of cellular activation on surface FcμR expression, blood MNCs were activated with various stimuli. Treatments of blood B cells with anti-μ mAb or PMA for 24 h resulted in an ~2.2-fold increase in the cell-surface FcμR level in comparison to that on B cells cultured in media only (unpublished data). In contrast, treatment of blood T cells with anti-CD3 mAb or PMA for 24–72 h reduced the cell-surface FcμR level by ~90%, suggesting that signaling through antigen receptors on B and T cells has distinct modulating effects on FcμR expression. Consistent with previous observations (Ferrarini et al., 1977; Pichler and Knapp, 1977; Sanders et al., 1987), there was enhanced FcμR expression by CLL B cells from three randomly selected patient blood samples (Fig. S8). Collectively, these findings indicate that, in striking contrast to other FcRs, FcμR is predominantly expressed by cells of the adaptive immune system. Moreover, the cell-surface levels of FcμR

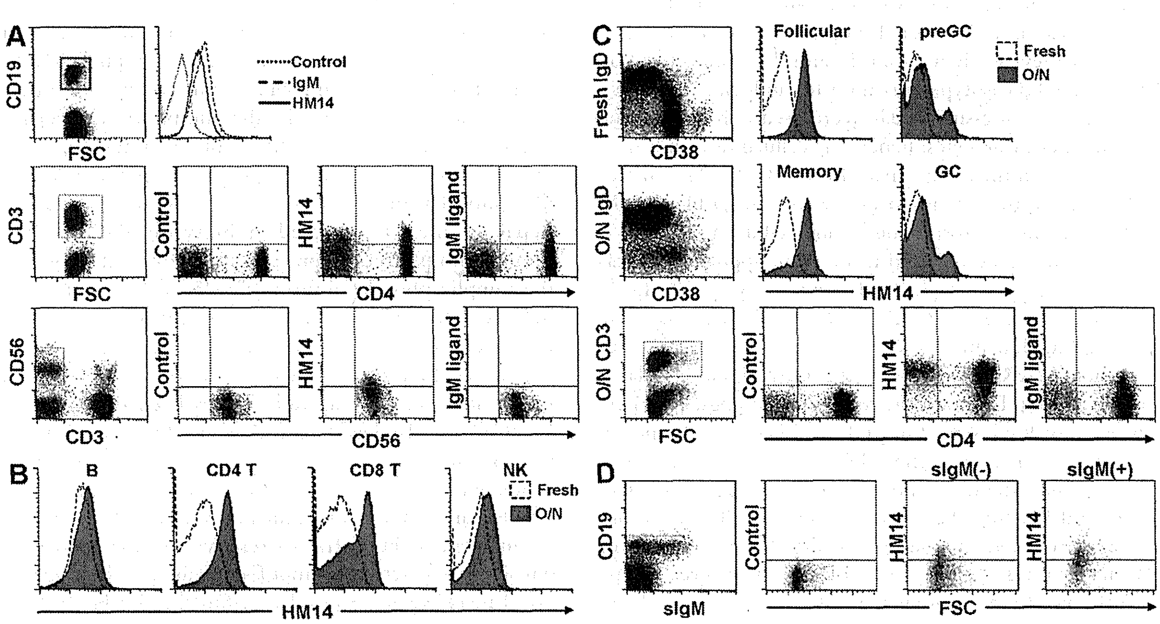

Figure 8. Immunofluorescence analysis of cell-surface FcμR expression in various tissues. (A–D) MNCs from blood (A and B), tonsils (C), and bone marrow (D) were first incubated with aggregated human IgG to block FcγRs and then with biotin-labeled HM14 anti-FcμR mAb along with the appropriate fluorochrome-labeled mAbs specific for CD19, IgM, IgD, CD38, CD3, CD4, CD8, or CD56. For IgM ligand binding, mouse IgMκ and biotin-labeled rat anti-mouse κ mAbs were sequentially added to MNCs without preincubation with aggregated IgG. The bound biotin-labeled reagents were detected by addition of SA-PE. Essentially the same results were obtained with the HM7 anti-FcμR mAb (not depicted). Because the results of the FcμR expression by CD3+/CD8+ and CD3+/CD4− T cells were essentially the same, the CD8 data were omitted for simplicity. The cell populations indicated by the red boxes were gated and examined for their reactivity with the HM14 anti-FcμR mAb and IgM ligand. Biotin-labeled irrelevant mAbs of the γ1κ (for HM14) or γ2bκ (for HM7) isotype were used as controls. The analysis was performed with freshly prepared cell preparations (A and D; labeled Fresh) or with cells cultured overnight in IgM-free media (O/N; B and C). Because the immunofluorescence profiles of freshly prepared tonsillar B cells with anti-FcμR mAbs and isotype-matched control mAbs as well as these of overnight-cultured B cells with the isotype-matched control mAbs were all essentially the same, only the results of freshly prepared and overnight-cultured B cells with anti-FcμR mAbs are shown in C (top) for simplicity. CD19+ B cells in tonsils (C) were analyzed for FcμR expression as follicular/naive (IgD+/CD38−), pregerminal center (preGC; IgD+/CD38+), germinal center (GC; IgD−/CD38+), and memory (IgD−/CD38−) cells. The frequency (%) of FcμR+ cells in each cell type among 10 different blood samples was 62 ± 18 for CD19+ B cells, 62 ± 13 for CD4+ T cells, 43 ± 23 for CD8+ T cells, and 19 ± 11 for CD56+ NK cells (means ± SD). The frequencies (%) of FcμR+ cells over the background staining with isotype-matched control mAbs in three tonsillar samples were 31 ± 7 for follicular/naive, 15 ± 3 for preGC, 10 ± 3 for GC, and 30 ± 12 for memory B cells, and 34 ± 6 for CD4+ T and 51 ± 7 for CD8+ T cells (means ± SD). The experiments were performed >10 times for A and B, 3 times for C, and 2 times for D.

are sensitive to IgM ligand concentration, tissue milieu, and cellular activation status.

DISCUSSION

We have identified for the first time a bona fide FcμR cDNA in humans. By using receptor-specific mAbs and IgM ligands, FcμR is defined as an ~60-kD transmembrane sialoglycoprotein. Its predicted structure consists of a single V-set Ig-like domain with homology to the Ig-binding domains of pIgR and Fcα/μR, an additional extracellular region with no known domain features, a transmembrane segment containing a charged His residue, and a relatively long cytoplasmic tail carrying conserved Tyr and Ser residues. Pentameric IgM and its $Fc_5\mu$ fragments bound cell-surface FcμR on transductants, but the Fabμ fragments and other Ig isotypes did not, thereby confirming the Fcμ specificity of this receptor. The affinity of the FcμR for its IgM ligand is strikingly high, ~10 nM. Despite the initial designation of FcμR as an antiapoptotic protein FAIM3/TOSO, FcμR per se had no inhibitory activity in Fas-mediated apoptosis, and such inhibition was only achieved when agonistic anti-Fas antibody of an IgM but not IgG isotype was used for inducing apoptosis. The cell types expressing FcμR were predominantly B and T cells and not phagocytes; hence, the cellular distribution of FcμR is quite distinct from that of other FcRs. The surface FcμR levels on those lymphocytes were susceptible to IgM ligand concentration, tissue milieu. and cellular activation.

The *FCMR* gene is found to be in an appropriate location on chromosome 1q32.2 adjacent to two other IgM-binding receptor genes (*PIGR* and *FCAMR*). Although the ligand-binding domains of these three receptors are similar to each other, FcμR seems to be the most distantly related among the group based on the following findings. (a) Many residues are well conserved in pIgR and Fcα/μR but not in FcμR. (b) The length of the CDR1 region, which is predicted to contact the Ig ligands, is shorter in FcμR (5 aa) than in pIgR and Fcα/μR (9 aa). (c) Within the CDR1 region, there are two charged residues: Arg31 conserved in both pIgR and Fcα/μR, and His32 conserved in all three receptors. Although Arg31 is predicted to be solvent exposed and to interact directly with polymeric IgA (Hamburger et al., 2004), FcμRs from seven different species have a noncharged residue at the corresponding position. (d) FcμR recognizes only the IgM isotype, whereas both pIgR and Fcα/μR in humans bind polymeric IgA and IgM (Kaetzel, 2005; Kikuno et al., 2007). These findings thus suggest that the interaction of FcμR with its IgM ligand is distinct from that of pIgR and Fcα/μR with IgM and polymeric IgA. In this regard, the finding that $Fc_5\mu$ fragments mostly consisting of the Cμ3/Cμ4 domains inhibit IgM binding to FcμR suggests that FcμR recognizes a molecular configuration on IgM that is conferred by the Cμ3/Cμ4 domains. In contrast, pIgR recognizes the C-terminal domain Cμ4 (Kaetzel, 2005).

The finding that the FcμR cDNAs identified in two cDNA libraries from PMA-activated 697 pre–B cells and CLL B cells encode a transmembrane but not a GPI-linked protein was unexpected, because in our previous biochemical analysis, the FcμR expressed on such pre–B cells was sensitive to GPI-PLC, whereas the FcμR on blood T cells was resistant (Ohno et al., 1990; Nakamura et al., 1993). An intensive search for an alternatively spliced transcript encoding a GPI-linked form of FcμR was unsuccessful but led to identification of an FcμR splice variant lacking the transmembrane exon that may encode a soluble form of FcμR with an M_r of ~34 kD (unpublished data). Reexamination of the susceptibility of FcμR to GPI-PLC treatment yielded an unequivocal result: the expression of FcμR on both PMA-activated 697 pre–B cells and T cell transductants was unchanged after GPI-PLC treatment, whereas the surface expression of GPI-anchored CD73 or Thy-1/CD90 was reduced by 50–65%. Thus, the discrepancy is likely caused by the fact that the GPI-PLC available for our studies in 1990 contained residual contaminating protease activity.

Unlike other FcRs, the FcμR has a relatively long cytoplasmic tail containing three conserved tyrosine and five to nine conserved serine residues. We found that some of these tyrosine and serine residues are targets for phosphorylation after FcμR ligation with IgM immune complexes or pervanadate treatment. Intriguingly, the phosphorylated FcμR was found to migrate on SDS-PAGE faster than the unphosphorylated form. One possible explanation for this is that such phosphorylation may cause a global structural change of FcμR leading to increased mobility on SDS-PAGE. Although phosphorylated proteins usually migrate slower than their unphosphorylated forms, CD45 on a myeloid cell line in fact exhibits enhanced mobility on SDS-PAGE after PMA-induced phosphorylation (Buzzi et al., 1992). Another explanation may be proteolytic cleavage in the cytoplasmic tail of FcμR after receptor ligation, as has been observed in the FcγRIIA on platelets (Gardiner et al., 2008). FcγRIIA ligation on platelets leads to activation of both the metalloprotease that targets the collagen receptor GPVI to shed its ectodomain and the intracellular calpain that cleaves the cytoplasmic tail of FcγRIIA to remove the immunoreceptor tyrosine-based activation motif–containing stub, suggesting a novel mechanism for platelet dysfunction by FcγRIIA after immunological insult including IgG autoantibodies to platelets. The precise mechanism for the enhanced migration of phosphorylated FcμR awaits further investigation.

Nucleotide sequence analysis indicated that FcμR and FAIM3/TOSO are identical, but we have clearly shown that the antiapoptotic activity of FcμR in Fas-bearing Jurkat cells is only observed when agonistic anti-Fas mAb of an IgM but not IgG_3 isotype is used and that the FcμR expression itself does not prevent Fas-mediated apoptosis. Addition of a 100-fold molar excess of control IgM into these cultures did not convert the $Fc\mu R^+GFP^+$ cells from resistance to sensitivity to IgM anti-Fas mAb–induced apoptosis. Even when FcμR and Fas on $Fc\mu R^+$ cells were brought into close physical proximity by ligation with a common secondary antibody, FcμR did not inhibit Fas-mediated apoptosis. Notably, Hitoshi et al. (1998) found that a FAIM3/TOSO deletion mutant lacking most of its cytoplasmic tail could still inhibit apoptosis mediated by IgM anti-Fas mAb, implying that FAIM3/TOSO might act indirectly through noncovalent association with another cell-surface protein. This might be relevant to our finding that an additional membrane protein of ~40 kD often coprecipitated with the ~60-kD FcμR from membrane lysates of $FcμR^+$ cells and that there is a charged His residue, which could be involved in electrostatic association with other proteins, adjacent to the transmembrane segment of FcμR. We therefore propose that the original designation of this gene as *FAIM3/TOSO* should be reconsidered and that renaming it *FCMR* would be more appropriate in keeping with its true physiological role.

Another reason to rename this gene is that several groups (Pallasch et al., 2008; Proto-Siqueira et al., 2008) have recently reported that *FAIM3/TOSO* is overexpressed in CLL, a heterogeneous leukemia thought to originate from antigen-stimulated B cells that escape normal cell-death mechanisms. The interpretation of this finding by both groups is that the resistance of CLL B cells to death mechanisms may result from the enhanced expression of "antiapoptotic" FAIM3/TOSO molecules. However, enhanced FcμR expression by CLL B cells had been consistently observed by many investigators using either rosetting or immunofluorescence methods (Ferrarini et al., 1977; Pichler and Knapp, 1977; Sanders et al., 1987). Although the mechanism for enhanced FcμR expression on CLL cells is unclear, it may result from chronic antigenic stimulation as supported by (a) reduced levels of membrane IgM, IgD, and CD79/Igα/Igβ on CLL cells and (b) polyreactivity of CLL-derived IgM molecules (Chiorazzi et al., 2005). In this regard, our finding that treatment of normal blood B cells with anti-μ antibody down-modulates membrane IgM and up-regulates FcμR cell-surface expression is consistent with the hypothesis that CLL cells are being activated by certain common antigens; thereby, antigen-driven proliferation may provide an alternative mode of survival of the leukemic cells.

The finding that the major cell types expressing FcμR are the adaptive immune cells, both B and T lymphocytes, is remarkable, because FcRs for the switched Ig isotypes (FcγRs, FcεRI, and FcαR) are expressed by various hematopoietic cells, including phagocytes, and are thought to be central mediators coupling the innate and adaptive immune responses (Nimmerjahn and Ravetch, 2008). Intriguingly, FcμR is the only FcR constitutively expressed on T cells, which are generally negative for the expression of other FcRs. The expression of FcμR by both $CD4^+$ and $CD8^+$ T cells is consistent with an early report that T cells forming rosettes with IgM-coated erythrocytes included both cell types (Reinherz et al., 1980). For B cells, FcμR is the only IgM-binding receptor expressed. Although the initial report indicated that Fcα/μR is expressed on B cells (Shibuya et al., 2000), our subsequent analyses revealed that the major cell type expressing Fcα/μR was a follicular dendritic cell in both humans (Kikuno et al., 2007) and mice (unpublished data). A small subpopulation of blood $CD56^+/CD3^-$ NK cells was also found to express FcμR, consistent with the results previously reported by others (Pricop et al., 1993; Rabinowich et al., 1996). The physiological relevance of such restricted cellular expression of FcμR may be related to unique features of the IgM ligand, such as its early appearance during immune responses, the pentameric configuration of its secreted form, and its potency in complement activation.

Many investigators had previously noticed the instability of IgM binding by B, T, and NK cells (Moretta et al., 1977; Nakamura et al., 1993; Pricop et al., 1993). We also found that the cell-surface FcμR levels were sensitive to extracellular IgM concentration, tissue milieu, and cellular activation status. This vulnerability could explain why FcμR was limited to an operationally defined entity for such a long time. As is the case with many other receptors, the detection of FcμR with IgM ligands was much less efficient than with anti-FcμR mAbs. Short-term culture in IgM-free media enhanced the cell-surface expression of FcμR on T cells and, to a lesser extent, on B and NK cells. Remarkably, this phenomenon was much more pronounced with cells from tonsils and spleen; cell-surface FcμR was not detectable on freshly isolated B and T cells from these organs but easily demonstrated after overnight culture in IgM-free media. Many other cell-surface antigens were detectable in those freshly isolated preparations, ruling out an artifact of tissue manipulation. To our knowledge, the IgM concentration in the interstitial spaces of such intact tissues has never been determined. If this in vivo down-modulation of FcμR is solely dependent on the extracellular concentration of IgM and not on the tissue microenvironment (e.g., proteases) or cellular activation status, then the interstitial IgM concentration in secondary lymphoid tissues is perhaps higher than in blood. In this regard, it is noteworthy that IgM-producing plasma cells are in the immediate vicinity of B and T cells within these lymphoid tissues.

Although both B and T cells express FcμR, there is a striking difference in their response after antigen receptor ligation. FcμR expression on B cells was up-regulated after treatment with anti-μ mAb, whereas its expression on T cells was down-modulated after treatment with anti-CD3 mAb. The response to PMA was also different in the B and T cells, suggesting that the difference might be attributed to the downstream events involving PKC. The role of PKC in internalization of cell-surface receptors including TCR has been clearly demonstrated (Cantrell et al., 1985; Minami et al., 1987; Bonefeld et al., 2003). PKC is a conserved family of 11 serine/threonine protein kinases, and most cell types express multiple isozymes of PKC (Spitaler and Cantrell, 2004). PKC α, β, δ, ε, η, θ, and ζ are known to be present in lymphocytes. Interestingly, the disruption of the gene encoding a single PKC isozyme expressed in both B and T cells (e.g., $PKC\beta^{-/-}$, $PKC\zeta^{-/-}$, and $PKC\delta^{-/-}$) often caused a selective immunological abnormality in only one of the cell types, suggesting compensatory or complementary functions of other PKC isozymes in the other cell type (Spitaler and Cantrell, 2004). Based on the consensus sequence motifs, there are several potential Ser residues available for phosphorylation by PKC in the human FcμR, particularly R-R-K-A-L-S283-R-R or A-P-S359-L-K. Thus, it seems possible that FcμR expressed on B and T cells may have distinct influences on their respective antigen receptor–mediated signaling.

With regard to the function of FcμR on B cells, it has been shown that passive administration of IgM antibody, in contrast to IgG, enhances the subsequent antibody response to relevant antigenic challenge (Hjelm et al., 2006). Recent studies with mice unable to produce the soluble form of IgM have clearly demonstrated the importance of secreted IgM in development of protective IgG antibody responses to viral and bacterial infections, presumably through both complement and FcμR systems (Boes et al., 1998a; Boes et al., 1998b; Ehrenstein et al., 1998; Ochsenbein et al., 1999; Baumgarth et al., 2000). The complement cleavage products C3dg and C3d attach covalently to antigen and cross-link both CD21 (CR2) and BCR on the membrane of B cells, thereby facilitating the B cell response to low concentrations of antigen despite the typically low affinity of BCR during the primary immune response (Fearon and Carter, 1995; Fearon and Carroll, 2000). The enhancing or adjuvant activity of C3d has been demonstrated with various antigens, although recently the inhibitory activity of C3d has also been reported for certain antigens (Bergmann-Leitner et al., 2006). Given that IgM antibody is a first line of host defense, it is reasonable to propose that FcμR may contribute to enhancement of B cell responses by interacting with BCR and CD21/CD19/CD81 via IgM–antigen–C3d complexes. Another potential role for FcμR on B cells is antigen presentation. The functional significance of FcμR on T cells has been the subject of considerable speculation (Moretta et al., 1977; Mathur et al., 1988b; Nakamura et al., 1993). It seems possible that FcμR on T cells may interact with the IgM BCR or IgM/antigen complexes on B cells to facilitate T and B cell interactions, thereby enhancing B cell activation. FcμR may also trigger cytotoxic T cells in IgM antibody–dependent cell-mediated cytotoxicity. The true physiological roles of FcμR, however, will become apparent with further studies, including analysis of the immunological phenotypes in FcμR-deficient mice. Although the molecular nature of the FcμR has long been elusive, its final unveiling in this study reveals a receptor full of intriguing aspects and opens new avenues of investigation.

MATERIALS AND METHODS

Construction of retroviral cDNA libraries. The cDNA libraries were constructed by a cDNA synthesis kit (Agilent Technologies) using poly(A)$^+$ RNA isolated by an Oligotex mRNA purification kit (QIAGEN) from (a) blood MNCs from a patient with CLL and (b) the 697 pre–B cell line preactivated with 10 nM PMA for 8 h, as previously described (Kubagawa et al., 1997). The *Eco*RI/*Xho*I-digested and size-fractionated cDNAs were ligated into the pMXsΔN/S retrovirus vector, in which the 1,328-bp *Not*I/*Sal*I fragment containing an IRES and a GFP cDNA was removed from the original pMXsIG vector (Kitamura et al., 2003). The ligated cDNA constructs were used to transform XL2-Blue MRF′ ultracompetent cells (Agilent Technologies). The titer of the cDNA library was ~10^5 and ~10^6 CFU/μg mRNA for CLL and 697 pre–B cells, respectively, and the mean size of the insert DNA in these libraries was ~1.6 kb.

Transfection, transduction, and screening. The cDNA libraries were transfected into the ecotropic retroviral packaging cell line BOSC23 with FuGENE 6 (Roche). 2 d later, the culture supernatants containing viruses were collected and filtered, and polybrene (Sigma-Aldrich) was added to a final concentration of 10 μg/ml before infecting the mouse thymoma line BW5147 at a ratio of ~3 × 10^5 cells/ml of supernatants. After 2 d, infected BW5147 T cells were incubated with biotin-labeled human IgMκ and then with antibiotin microbeads (Miltenyi Biotec) or PE-labeled SA (SouthernBiotech) before sorting IgM-binding cells by MACS or FACS, respectively. Enrichment of IgM-binding cells was repeated three times for MACS and once for FACS within the interval of ~3 d, and the final FACS-sorted cells were cloned by limiting dilution.

Identification of cDNA inserts and sequencing. Total RNA isolated from single-cell derived, IgM-binding and -nonbinding subclones was converted to first-strand cDNA with a primer (5′-CCCTTTTTCTGGAGACTAAAT-3′) corresponding to the 3′ vector sequence flanking the cloning site and SuperScript II RT (Invitrogen). The resultant first-strand cDNAs were used as template DNAs in PCR amplification with PrimeSTAR HS DNA polymerase (Takara Bio Inc.) and a set of primers corresponding to the 5′ and 3′ flanking vector sequences of the cloning site, as previously described (Arase et al., 2001). Amplified PCR products were subcloned into the ZeroBlunt TOPO vector (Invitrogen) before sequencing analysis was performed at our institutional sequencing core facility using a DNA analyzer (model 3730xl) and DNA Sequencing Analysis Software (version 5.2; both from Applied Biosystems).

Preparation of FcμR stable transductants. Total RNAs isolated from PMA-activated 697 pre–B cells, CLL B cells, and tonsils were similarly converted to first-strand cDNA with an oligo(dT)$_{18}$ primer, and the resultant first-strand cDNAs were used as template DNAs for amplification of FcμR cDNA with a set of primers (forward, 5′-AGATCTAGAAGGGACAATGGACT-3′, and reverse, 5′-GAATTCTCAGGCAGGAACATTGATGT-3′; underlined portions indicate *Bgl*II and *Eco*RI sites). Amplified products of the expected size of ~1.2 kb were subcloned into the *Bam*HI and *Eco*RI sites of the pMXsPIE retroviral vector that contains a GFP cDNA and *Streptomyces alboniger* puromycin-*N*-acetyltransferase cDNA (a gift of A. Mui; DNAX, San Francisco, CA; Ehrhardt et al., 1999). After confirming sequence identity, the ligated FcμR cDNA construct and the empty vector were similarly transduced in BW5147 T cells, and the GFP$^+$ cells in both transductants were enriched by FACS and in the presence of 1 μg/ml puromycin. For FcμR$^+$ Jurkat cells, both the FcμR/GFP and GFP-only constructs were transfected into the 293T-A amphotropic packaging cell line before transducing the human Jurkat T cell line. GFP$^+$ cells were enriched three times by FACS before establishing the stable cell lines. In some experiments, both FcμR/GFP and GFP constructs were similarly transfected into an appropriate packaging cell line and transduced into WEHI231 mouse B cells and Ramos human B cells.

Ig ligands and binding assay. Human IgM myeloma proteins were purified from serum samples by euglobulin fractionation and Sephacryl S-300 gel filtration column chromatography (GE Healthcare; Ohno et al., 1990). The Fc$_5$μ and Fabμ fragments were prepared from a human IgMκ by hot trypsin digestion (Plaut and Tomasi, 1970; Ohno et al., 1990; Nakamura et al., 1993). Other human myeloma Igs of each isotype (γ1, γ2, γ3, γ4, α1, α2, δ, and ε) and mouse myeloma IgM were purchased from EMD and Sigma-Aldrich. The purity of IgM, its fragments, and other myeloma Igs was confirmed by SDS-PAGE under both reducing and nonreducing conditions. Protein concentration was determined by absorbance at 280 nm with an extinction coefficient of 1.4 as 1 mg/ml. For the binding inhibition assay, FcμR$^+$ BW5147 T cells were incubated with various concentrations of Ig preparations along with a constant amount of biotin-labeled IgMκ, washed, and incubated with PE-labeled SA to determine the bound IgM.

Production of hybridoma mAbs. BALB/c mice were hyperimmunized subcutaneously with BW5147 T cells expressing human FcμR, and regional lymph node cells were fused with the Ag8.653 plasmacytoma line, as previously described (Kikuno et al., 2007). Hybridoma clones producing IgG mAbs reactive with FcμR$^+$ BW5147 T cells, but not with Fcα/μR$^+$ BW5147 T cells, control BW5147 T cells, and pIgR$^+$ FT-29 cells were selected and subcloned by limiting dilution. Two human FcμR-specific mAbs, HM7 (γ2bκ) and HM14 (γ1κ), were selected in this study. Their F(ab')$_2$ fragments were prepared by digestion with lysyl endopeptidase (Yamaguchi et al., 1995) and pepsin (Maruyama et al., 1985) for HM7 and HM14, respectively.

Flow cytometric analysis of cells. Blood MNCs were isolated by Ficoll-Hypaque density gradient centrifugation. Granulocytes were isolated from erythrocyte pellets by differential sedimentation in 1.5% dextran in PBS. MNCs were also prepared from long bone, tonsil, and spleen tissues obtained from our institutional tissue procurement service. Approval for use of these human materials in this investigation was obtained from the University of Alabama at Birmingham Institutional Review Board. Cells were first incubated with aggregated human IgG to block FcγRs and then stained with biotin-labeled anti-FcμR mAbs along with fluorochrome-labeled mAbs specific for CD3, CD4, CD8, CD19, CD14, CD56, CD10, or CD13. PE-labeled SA was used as a developing reagent for biotinylated mAbs. Controls included isotype-matched irrelevant mAbs labeled with the corresponding fluorochromes or biotin. In some experiments, biotin-labeled F(ab')$_2$ fragments of anti-FcμR mAbs were used. Stained cells were analyzed with a FACSCalibur instrument (BD). For GPI-PLC treatment, 10^6 cells were incubated for 45 min at 30°C in 10 mM Hepes/HBSS (without Ca^{2+} and Mg^{2+}) containing 10 U/ml GPI-PLC (Sigma-Aldrich). After treatment, cells were washed and examined for FcμR and other cell-surface antigens by FACSCalibur. For neuraminidase treatment, 5×10^6 cells/ml in HBSS were incubated with 50 U/ml neuraminidase (New England Biolabs, Inc.) at 37°C for 45 min before washing and immunofluorescence analysis.

Cell-surface biotinylation and immunoprecipitation analysis. Plasma membrane proteins on 10^7 viable cells were labeled with 1 ml sulfo-NHS-LC-biotin (0.1 mg/ml; Thermo Fisher Scientific) in 0.15 M NaCl/0.1 M Hepes (pH 8) for 30 min at 25°C. After washing, biotinylated cells were incubated with 10 μl anti-FcμR or isotype-matched control mAbs or mouse IgMκ ligand (50 μg/ml) for 20 min on ice, washed, and lysed in 200 μl of 1% NP-40 lysis buffer containing protease inhibitors (Sanders et al., 1987; Ohno et al., 1990; Nakamura et al., 1993). Cleared lysates were either transferred to 96-well plates precoated with 20 μg/ml of rat anti–mouse κ mAb (clone 187.1; Yelton et al., 1981) or incubated with rat anti–mouse κ mAb–coupled beads, and the bound materials were dissociated and separated by SDS-PAGE under reducing and nonreducing conditions, followed by transfer to membranes, blotting with horseradish peroxidase (HRP)–SA, and visualization by ECL (GE Healthcare), as previously described (Kikuno et al., 2007). In some experiments, the anti-FcμR mAb–bound materials were resuspended in 7 M urea/2 M thiourea/4% CHAPS/40 mM dithiothreitol/0.5% ampholite (pH 3–10)/40 mM Tris-HCl (pH 8.8) and subjected to two-dimensional gel electrophoresis analysis, as previously described (Ohno et al., 1990).

Immunoblot analysis. To determine the phosphorylation status of Tyr and Ser residues in FcμR, 3×10^7 cells serum starved for 1.5 h in RPMI 1640/20 mM Hepes media were treated with 100 μM pervanadate for 15 min at 37°C, lysed in 1 ml of 1% NP-40 lysis buffer with protease/phosphatase inhibitors, and immunoprecipitated with Sepharose 4B beads coupled to HM14 anti-FcμR mAb or AM3 anti-Fcα/μR mAb as an isotype-matched control. The bound materials were dissociated with 0.1 M glycine-HCl buffer (pH 2.8) in 0.5% NP-40, immediately neutralized with 1 M Tris, and resolved on SDS–10% PAGE before transfer onto membranes. After soaking with 5% nonfat milk, membranes were immunoblotted with HRP-labeled antiphosphotyrosine mAb (4G10; Millipore) or rabbit antibody specific for phosphoserine of PKC substrates (Cell Signaling Technology) along with HRP-labeled goat anti–rabbit Ig antibody (SouthernBiotech) as a developing reagent. For receptor ligation, serum-starved cells were incubated with 50 μl of the preformed IgM immune complexes, an equal mixture of human IgMκ myeloma protein (100 μg/ml) and F(ab')$_2$ fragments of anti–human μ mAb with specificity for the Cμ1 domain (50 μg/ml), at 37°C for 0, 3, and 30 min before solubilizing in 200 μl of 1% NP-40 lysis buffer. The cleared lysates were subjected to immunoprecipitation with HM14 or AM3 mAb–coupled beads, and the bound materials were similarly analyzed by immunoblotting. Immunoblotted membranes were visualized by ECL. After dissociating the blotting antibodies, the membranes were reblotted with biotin-labeled anti-FcμR mAbs (HM14 and HM7) to confirm the phosphorylation of Tyr and Ser residues of FcμR.

Apoptosis assay. 4×10^5 cells/ml were cultured for 24 h in RPMI 1640 containing 10% FCS, penicillin/streptomycin, and 5×10^{-5} M 2-ME in the presence or absence of either of the agonistic anti-Fas mAbs, CH11 (10 ng/ml; mouse μk isotype; Millipore) or 2R2 (300 ng/ml; mouse γ3κ; Invitrogen), washed twice with PBS, and incubated with 7-AAD and allophycocyanin (APC)-labeled annexin V for detecting apoptotic cells according to the manufacturer's recommendation (BD). In some experiments, 100-fold molar excess of human or mouse IgM myeloma protein as a ligand was added in these cultures. In other experiments, cells were preincubated with the 2R2 anti-Fas mAb (300 ng/ml) and either F(ab')$_2$ fragments or the intact form of the HM14 anti-FcμR mAb (50 μg/ml) for 20 min at 4°C, washed, and cultured in the presence or absence of F(ab')$_2$ fragments of goat anti–mouse κ antibodies (50 μg/ml) overnight at 37°C.

Scatchard plot analysis. 2×10^6 FcμR$^+$ BW5147 T cells were incubated in triplicate with serial dilutions of ^{125}I-labeled IgM with a specific activity of ~1.6×10^{17} cpm/mol in 30 μl PBS containing 3% FCS and 0.2% sodium azide for 1.5 h at room temperature before washing and aspirating unbound IgM by centrifugation. Some tubes contained a 200-fold molar excess of cold IgM to determine the amounts of nonspecific binding of ^{125}I-labeled IgM to cells. The numbers of IgM molecules specifically bound per cell were plotted on the x axis against the ratio of bound to free IgM on the y axis, and the apparent dissociation constant was obtained by dividing the number of receptors per cell by the bound/free ratio at the y-axis intercept, as previously described (Lowenthal et al., 2001).

Online supplemental material. Fig. S1 shows the nucleotide sequence of the human FcμR cDNA. Fig. S2 shows the definition of FAIM3/TOSO as an FcμR. Fig. S3 shows the predicted protein structure of human FcμR. Fig. S4 shows the effects of FcμR ligation on anti-Fas antibody–mediated apoptosis in Jurkat T cells. Fig. S5 shows the expression of cell-surface FcμR on 697 pre-B cell line before and after PMA stimulation. Fig. S6 shows *FCMR* gene expression analyzed by RT-PCR. Fig. S7 shows the lack of FcμR expression by monocytes, granulocytes, erythrocytes, and platelets. Fig. S8 shows enhanced FcμR expression on CLL cells. Online supplemental material is available at http://www.jem.org/cgi/content/full/jem.20091107/DC1.

This paper is dedicated to our former friends and FcμR investigators, E.W. Lamon and C.E. Grossi.

We thank S. Izui, S.K. Sanders, I.C.M. MacLennan, T. Kawakami, and S.J. Frank for valuable suggestions; T. Motohashi and A. Sasada for excellent technical support; P.D. Burrows and J.E. Volanakis for critically reading the manuscript; M.G. Salazar for DNA sequencing (AI27767); H. Kim and G.D. Robinson for two-dimensional gel electrophoresis (CA13148); our institutional tissue procurement staff for providing human tissues (CA13148); D.W. Garber, J. Novak, R.T. Brown, and J.K. Adams for providing the facility for iodination experiments; and J.B. Bennett for manuscript preparation. E. Takayama, T. Kitamura, and H. Kubagawa set up the retroviral expression procedure; H. Kubagawa and I. Torii cloned the FcμR cDNA; H. Kubagawa and D.-W. Kang produced anti-FcμR mAbs; S. Oka performed immunofluorescence assays; Y. Kubagawa and H. Kubagawa conducted biochemical and signaling analyses; H. Kubagawa, S. Oka, H. Mori, and J.-Y. Wang performed apoptosis experiments; H. Takatsu and H. Ohno performed mouse FcμR expression analysis; G.L. Gartland performed the FACS sort; L.F. Bertoli provided CLL patients' materials; and H. Kubagawa wrote the manuscript.

This work was supported in part by National Institute of Allergy and Infectious Diseases/National Institutes of Health grants AI52243 and AI42127 (to H. Kubagawa).

The authors have no conflicting financial interests.

Submitted: 21 May 2009
Accepted: 25 September 2009

REFERENCES

Arase, H., T. Saito, J.H. Phillips, and L.L. Lanier. 2001. Cutting edge: the mouse NK cell-associated antigen recognized by DX5 monoclonal antibody is CD49b (α 2 integrin, very late antigen-2). *J. Immunol.* 167:1141–1144.

Basten, A., N.L. Warner, and T. Mandel. 1972. A receptor for antibody on B lymphocytes. II. Immunochemical and electron microscopy characteristics. *J. Exp. Med.* 135:627–642. doi:10.1084/jem.135.3.627

Baumgarth, N., O.C. Herman, G.C. Jager, L.E. Brown, L.A. Herzenberg, and J. Chen. 2000. B-1 and B-2 cell–derived immunoglobulin M antibodies are nonredundant components of the protective response to influenza virus infection. *J. Exp. Med.* 192:271–280. doi:10.1084/jem.192.2.271

Bergmann-Leitner, E.S., W.W. Leitner, and G.C. Tsokos. 2006. Complement 3d: from molecular adjuvant to target of immune escape mechanisms. *Clin. Immunol.* 121:177–185. doi:10.1016/j.clim.2006.07.001

Boes, M., C. Esau, M.B. Fischer, T. Schmidt, M. Carroll, and J. Chen. 1998a. Enhanced B-1 cell development, but impaired IgG antibody responses in mice deficient in secreted IgM. *J. Immunol.* 160:4776–4787.

Boes, M., A.P. Prodeus, T. Schmidt, M.C. Carroll, and J. Chen. 1998b. A critical role of natural immunoglobulin M in immediate defense against systemic bacterial infection. *J. Exp. Med.* 188:2381–2386. doi:10.1084/jem.188.12.2381

Bonefeld, C.M., A.B. Rasmussen, J.P. Lauritsen, M. von Essen, N. Ødum, P.S. Andersen, and C. Geisler. 2003. TCR comodulation of nonengaged TCR takes place by a protein kinase C and CD3 γ di-leucine-based motif-dependent mechanism. *J. Immunol.* 171:3003–3009.

Buzzi, M., L. Lu, A.J. Lombardi Jr., M.R. Posner, D.L. Brautigan, L.D. Fast, and A.R. Frackelton Jr. 1992. Differentiation-induced changes in protein-tyrosine phosphatase activity and commensurate expression of CD45 in human leukemia cell lines. *Cancer Res.* 52:4027–4035.

Cantrell, D.A., A.A. Davies, and M.J. Crumpton. 1985. Activators of protein kinase C down-regulate and phosphorylate the T3/T-cell antigen receptor complex of human T lymphocytes. *Proc. Natl. Acad. Sci. USA.* 82:8158–8162. doi:10.1073/pnas.82.23.8158

Chiorazzi, N., K.R. Rai, and M. Ferrarini. 2005. Chronic lymphocytic leukemia. *N. Engl. J. Med.* 352:804–815. doi:10.1056/NEJMra041720

Conrad, D.H. 1990. FcεRII/CD23: the low affinity receptor for IgE. *Annu. Rev. Immunol.* 8:623–645.

Ehrenstein, M.R., T.L. O'Keefe, S.L. Davies, and M.S. Neuberger. 1998. Targeted gene disruption reveals a role for natural secretory IgM in the maturation of the primary immune response. *Proc. Natl. Acad. Sci. USA.* 95:10089–10093. doi:10.1073/pnas.95.17.10089

Ehrhardt, G.R., K.B. Leslie, F. Lee, J.S. Wieler, and J.W. Schrader. 1999. M-Ras, a widely expressed 29-kD homologue of p21 Ras: expression of a constitutively active mutant results in factor-independent growth of an interleukin-3-dependent cell line. *Blood.* 94:2433–2444.

Fearon, D.T., and M.C. Carroll. 2000. Regulation of B lymphocyte responses to foreign and self-antigens by the CD19/CD21 complex. *Annu. Rev. Immunol.* 18:393–422. doi:10.1146/annurev.immunol.18.1.393

Fearon, D.T., and R.H. Carter. 1995. The CD19/CR2/TAPA-1 complex of B lymphocytes: linking natural to acquired immunity. *Annu. Rev. Immunol.* 13:127–149. doi:10.1146/annurev.iy.13.040195.001015

Ferrarini, M., T. Hoffman, S.M. Fu, R. Winchester, and H.G. Kunkel. 1977. Receptors for IgM on certain human B lymphocytes. *J. Immunol.* 119:1525–1529.

Gardiner, E.E., D. Karunakaran, J.F. Arthur, F.T. Mu, M.S. Powell, R.I. Baker, P.M. Hogarth, M.L. Kahn, R.K. Andrews, and M.C. Berndt. 2008. Dual ITAM-mediated proteolytic pathways for irreversible inactivation of platelet receptors: de-ITAM-izing FcgammaRIIa. *Blood.* 111:165–174. doi:10.1182/blood-2007-04-086983

Haegert, D.G. 1979. Phagocytic peripheral blood monocytes from rabbits and humans express membrane receptors specific for IgM molecules: evidence that incubation with neuraminidase exposes cryptic IgM (Fc) receptors. *Clin. Exp. Immunol.* 35:484–490.

Hamburger, A.E., A.P. West Jr., and P.J. Bjorkman. 2004. Crystal structure of a polymeric immunoglobulin binding fragment of the human polymeric immunoglobulin receptor. *Structure.* 12:1925–1935. doi:10.1016/j.str.2004.09.006

Haury, M., A. Sundblad, A. Grandien, C. Barreau, A. Coutinho, and A. Nobrega. 1997. The repertoire of serum IgM in normal mice is largely independent of external antigenic contact. *Eur. J. Immunol.* 27:1557–1563. doi:10.1002/eji.1830270635

Hitoshi, Y., J. Lorens, S.I. Kitada, J. Fisher, M. LaBarge, H.Z. Ring, U. Francke, J.C. Reed, S. Kinoshita, and G.P. Nolan. 1998. Toso, a cell surface, specific regulator of Fas-induced apoptosis in T cells. *Immunity.* 8:461–471. doi:10.1016/S1074-7613(00)80551-8

Hjelm, F., F. Carlsson, A. Getahun, and B. Heyman. 2006. Antibody-mediated regulation of the immune response. *Scand. J. Immunol.* 64:177–184. doi:10.1111/j.1365-3083.2006.01818.x

Horejsí, V., W. Zhang, and B. Schraven. 2004. Transmembrane adaptor proteins: organizers of immunoreceptor signalling. *Nat. Rev. Immunol.* 4:603–616. doi:10.1038/nri1414

Kaetzel, C.S. 2005. The polymeric immunoglobulin receptor: bridging innate and adaptive immune responses at mucosal surfaces. *Immunol. Rev.* 206:83–99. doi:10.1111/j.0105-2896.2005.00278.x

Kikuno, K., D.W. Kang, K. Tahara, I. Torii, H.M. Kubagawa, K.J. Ho, L. Baudino, N. Nishizaki, A. Shibuya, and H. Kubagawa. 2007. Unusual biochemical features and follicular dendritic cell expression of human Fcα/μ receptor. *Eur. J. Immunol.* 37:3540–3550. doi:10.1002/eji.200737655

Kitamura, T., Y. Koshino, F. Shibata, T. Oki, H. Nakajima, T. Nosaka, and H. Kumagai. 2003. Retrovirus-mediated gene transfer and expression cloning: powerful tools in functional genomics. *Exp. Hematol.* 31:1007–1014.

Kubagawa, H., P.D. Burrows, and M.D. Cooper. 1997. A novel pair of immunoglobulin-like receptors expressed by B cells and myeloid cells. *Proc. Natl. Acad. Sci. USA.* 94:5261–5266. doi:10.1073/pnas.94.10.5261

Lamon, E.W., B. Andersson, H.D. Whitten, M.M. Hurst, and V. Ghanta. 1976. IgM complex receptors on subpopulations of murine lymphocytes. *J. Immunol.* 116:1199–1203.

Lowenthal, J.W., T.R. Malek, and H. Saragovi. 2001. Measurement of lymphokine receptors. *Curr. Protoc. Immunol.* 6:1–15.

Maruyama, S., H. Kubagawa, and M.D. Cooper. 1985. Activation of human B cells and inhibition of their terminal differentiation by monoclonal anti-μ antibodies. *J. Immunol.* 135:192–199.

Mathur, A., R.G. Lynch, and G. Köhler. 1988a. Expression, distribution and specificity of Fc receptors for IgM on murine B cells. *J. Immunol.* 141:1855–1862.

Mathur, A., R.G. Lynch, and G. Köhler. 1988b. The contribution of constant region domains to the binding of murine IgM to Fcμ receptors on T cells. *J. Immunol.* 140:143–147.

Minami, Y., L.E. Samelson, and R.D. Klausner. 1987. Internalization and cycling of the T cell antigen receptor. Role of protein kinase C. *J. Biol. Chem.* 262:13342–13347.

Moretta, L., M. Ferrarini, M.L. Durante, and M.C. Mingari. 1975. Expression of a receptor for IgM by human T cells in vitro. *Eur. J. Immunol.* 5:565–569. doi:10.1002/eji.1830050812

Moretta, L., S.R. Webb, C.E. Grossi, P.M. Lydyard, and M.D. Cooper. 1977. Functional analysis of two human T-cell subpopulations: help and suppression of B-cell responses by T cells bearing receptors for IgM or IgG. *J. Exp. Med.* 146:184–200. doi:10.1084/jem.146.1.184

Nakamura, T., H. Kubagawa, T. Ohno, and M.D. Cooper. 1993. Characterization of an IgM Fc-binding receptor on human T cells. *J. Immunol.* 151:6933–6941.

Nimmerjahn, F., and J.V. Ravetch. 2008. Fcγ receptors as regulators of immune responses. *Nat. Rev. Immunol.* 8:34–47. doi:10.1038/nri2206

Ochsenbein, A.F., T. Fehr, C. Lutz, M. Suter, F. Brombacher, H. Hengartner, and R.M. Zinkernagel. 1999. Control of early viral and bacterial distribution and disease by natural antibodies. *Science.* 286:2156–2159. doi:10.1126/science.286.5447.2156

Ohno, T., H. Kubagawa, S.K. Sanders, and M.D. Cooper. 1990. Biochemical nature of an Fcμ receptor on human B-lineage cells. *J. Exp. Med.* 172:1165–1175. doi:10.1084/jem.172.4.1165

Pallasch, C.P., A. Schulz, N. Kutsch, J. Schwamb, S. Hagist, H. Kashkar, A. Ultsch, C. Wickenhauser, M. Hallek, and C.M. Wendtner. 2008.

Overexpression of TOSO in CLL is triggered by B-cell receptor signaling and associated with progressive disease. *Blood.* 112:4213–4219. doi:10.1182/blood-2008-05-157255

Pichler, W.J., and W. Knapp. 1977. Receptors for IgM-coated erythrocytes on chronic lymphatic leukemia cells. *J. Immunol.* 118:1010–1015.

Plaut, A.G., and T.B. Tomasi Jr. 1970. Immunoglobulin M: pentameric Fcμ fragments released by trypsin at higher temperatures. *Proc. Natl. Acad. Sci. USA.* 65:318–322. doi:10.1073/pnas.65.2.318

Pricop, L., H. Rabinowich, P.A. Morel, A. Sulica, T.L. Whiteside, and R.B. Herberman. 1993. Characterization of the Fcμ receptor on human natural killer cells. Interaction with its physiologic ligand, human normal IgM, specificity of binding, and functional effects. *J. Immunol.* 151:3018–3029.

Proto-Siqueira, R., R.A. Panepucci, F.P. Careta, A. Lee, A. Clear, K. Morris, C. Owen, E.G. Rizzatti, W.A. Silva Jr., R.P. Falcão, et al. 2008. SAGE analysis demonstrates increased expression of TOSO contributing to Fas-mediated resistance in CLL. *Blood.* 112:394–397. doi:10.1182/blood-2007-11-124065

Rabinowich, H., M. Manciulea, D. Metes, A. Sulica, R.B. Herberman, S.J. Corey, and T.L. Whiteside. 1996. Physical and functional association of Fcμ receptor on human natural killer cells with the ζ- and FcεRI γ-chains and with src family protein tyrosine kinases. *J. Immunol.* 157:1485–1491.

Ravetch, J.V., and F. Nimmerjahn. 2008. Fc receptors and their role in immune regulation and inflammation. *In* Fundamental Immunology. Sixth edition. W.E. Paul, editor. Lippincott Williams & Wilkins, Philadelphia. 684–705.

Reinherz, E.L., L. Moretta, M. Roper, J.M. Breard, M.C. Mingari, M.D. Cooper, and S.F. Schlossman. 1980. Human T lymphocyte subpopulations defined by Fc receptors and monoclonal antibodies. A comparison. *J. Exp. Med.* 151:969–974. doi:10.1084/jem.151.4.969

Roopenian, D.C., and S. Akilesh. 2007. FcRn: the neonatal Fc receptor comes of age. *Nat. Rev. Immunol.* 7:715–725. doi:10.1038/nri2155

Sanders, S.K., H. Kubagawa, T. Suzuki, J.L. Butler, and M.D. Cooper. 1987. IgM binding protein expressed by activated B cells. *J. Immunol.* 139:188–193.

Santana, V. 1977. Receptors for IgM on murine lymphoid cells. *Immunology.* 32:273–278.

Shibuya, A., N. Sakamoto, Y. Shimizu, K. Shibuya, M. Osawa, T. Hiroyama, H.J. Eyre, G.R. Sutherland, Y. Endo, T. Fujita, et al. 2000. Fcα/μ receptor mediates endocytosis of IgM-coated microbes. *Nat. Immunol.* 1:441–446. doi:10.1038/80886

Spitaler, M., and D.A. Cantrell. 2004. Protein kinase C and beyond. *Nat. Immunol.* 5:785–790. doi:10.1038/ni1097

Thompson, J.D., D.G. Higgins, and T.J. Gibson. 1994. CLUSTAL W: improving the sensitivity of progressive multiple sequence alignment through sequence weighting, position-specific gap penalties and weight matrix choice. *Nucleic Acids Res.* 22:4673–4680. doi:10.1093/nar/22.22.4673

Tony, H.P., and A. Schimpl. 1980. Stimulation of murine B cells with anti-Ig antibodies: dominance of a negative signal mediated by the Fc receptor. *Eur. J. Immunol.* 10:726–729. doi:10.1002/eji.1830100914

Uher, F., I. Dobronyi, and J. Gergel. 1981. IgM-Fc receptor-mediated phagocytosis of rat macrophages. *Immunology.* 42:419–425.

Yamaguchi, Y., H. Kim, K. Kato, K. Masuda, I. Shimada, and Y. Arata. 1995. Proteolytic fragmentation with high specificity of mouse immunoglobulin G. Mapping of proteolytic cleavage sites in the hinge region. *J. Immunol. Methods.* 181:259–267. doi:10.1016/0022-1759(95)00010-8

Yelton, D.E., C. Desaymard, and M.D. Scharff. 1981. Use of monoclonal anti-mouse immunoglobulin to detect mouse antibodies. *Hybridoma.* 1:5–11.

Developmental Biology 337 (2010) 405–414

Contents lists available at ScienceDirect

Developmental Biology

journal homepage: www.elsevier.com/developmentalbiology

Cv2, functioning as a pro-BMP factor via twisted gastrulation, is required for early development of nephron precursors

Makoto Ikeya [a,*,1], Kumi Fukushima [a], Masako Kawada [a], Sachiko Onishi [b], Yasuhide Furuta [c], Shigenobu Yonemura [b], Toshio Kitamura [d], Tetsuya Nosaka [e], Yoshiki Sasai [a,*]

[a] Organogenesis and Neurogenesis Group, RIKEN Center for Developmental Biology, 2-2-3 Minatojima-minamimachi, Chuo, Kobe 650-0047, Japan
[b] Electron Microscope Laboratory, RIKEN Center for Developmental Biology, Kobe 650-0047, Japan
[c] Department of Biochemistry and Molecular Biology, M.D. Anderson Cancer Center, University of Texas, Houston, TX 77030, USA
[d] Division of Cellular Therapy, The Institute of Medical Science, University of Tokyo, Tokyo 108-8639, Japan
[e] Department of Microbiology, Mie University Graduate School of Medicine, Tsu, Mie 514-8507, Japan

ARTICLE INFO

Article history:
Received for publication 8 July 2009
Revised 8 November 2009
Accepted 9 November 2009
Available online 13 November 2009

Keywords:
BMP
Kidney
Organogenesis
Genetic interactions

ABSTRACT

The fine-tuning of BMP signals is critical for many aspects of complex organogenesis. In this report, we show that the augmentation of BMP signaling by a BMP-binding secreted factor, Crossveinless2 (Cv2), is essential for the early embryonic development of mammalian nephrons. In the *Cv2*-null mouse, the number of cap condensates (clusters of nephron progenitors, which normally express Cv2) was decreased, and the condensate cells exhibited a reduced level of aggregation. In these $Cv2^{-/-}$ condensates, the level of phosphorylated Smad1 (pSmad1) was substantially lowered. The loss of a *Bmp7* allele in the $Cv2^{-/-}$ mouse enhanced the cap condensate defects and further decreased the level of pSmad1 in this tissue. These observations indicated that Cv2 has a pro-BMP function in early nephrogenesis. Interestingly, the renal defects of the $Cv2^{-/-}$ mutant were totally suppressed by a null mutation of *Twisted gastrulation* (*Tsg*), which encodes another BMP-binding factor, showing that Cv2 exerts its pro-BMP nephrogenic function Tsg-dependently. By using an embryonic kidney cell line, we presented experimental evidence showing that Cv2 enhances pro-BMP activity of Tsg. These findings revealed the molecular hierarchy between extracellular modifiers that orchestrate local BMP signal peaks in the organogenetic microenvironment.

Introduction

In terrestrial amniotes, the kidney is an indispensable and complex organ that maintains fluid homeostasis and blood pressure. Its anlage is a tissue called the metanephros. In the mouse, metanephric development starts about embryonic day (E) 10.5 with the demarcation of the metanephric blastema in the caudal part of the intermediate mesoderm, followed by reciprocal inductions between the blastema and the Wolffian duct (Vainio and Lin, 2002). In response to metanephric blastema-derived signals, the ureteric bud forms from the Wolffian duct, invades the metanephric blastema, and successively branches to form the collecting ducts. Conversely, ureteric bud-derived signals induce the formation of metanephric blastema-derived condensates (cap condensates) around the tips of collecting ducts; the cells forming the condensates will ultimately give rise to the nephrons, which carry out the functions of the adult kidney (Kobayashi et al., 2008). Although the signaling networks that regulate duct branching have been extensively studied (Shah et al., 2004), relatively little is known about the molecular mechanism of how cap condensates are formed and maintained (Kobayashi et al., 2008; Oxburgh et al., 2004).

The Bone Morphogenetic Protein (BMP) family is a class of secreted signaling proteins that belong to the transforming growth factor-beta (TGFβ) superfamily; they have diverse effects on the control of embryogenesis, including kidney development (Cain et al., 2008; Godin et al., 1998; Hogan, 1996; Simic and Vukicevic, 2005). An intriguing feature of BMP signaling is the presence of various extracellular BMP inhibitors (i.e., anti-BMP factors), such as Chordin, Noggin, Follistatin, Cerberus, and Gremlin (Glinka et al., 1997; Hemmati-Brivanlou et al., 1994; Hsu et al., 1998; Lamb et al., 1993; Sasai et al., 1995, 1994; Smith and Harland, 1992). Moreover, recent studies show that there are some proteins that bind to BMPs extracellularly and augment their signaling (i.e., pro-BMP factors). One protein with pro-BMP functions is Crossveinless2 (Cv2; also called Bmper), which enhances BMP signaling during wing cross-vein formation in *Drosophila*, as well as in neural crest emigration in the chick embryo, dorsal-ventral patterning of the zebrafish gastrula, and some cultured cell lines (Coles et al., 2004; Conley et al., 2000; Kamimura et al., 2004; Kelley et al., 2009; Moser et al., 2007; Rentzsch et al., 2006; Serpe et al., 2008).

* Corresponding authors. Fax: +81 78 306 1854.
E-mail addresses: mikeya@cdb.riken.jp (M. Ikeya), yoshikisasai@cdb.riken.jp (Y. Sasai).
[1] Present address: Department of Cell Modulation, Institute of Molecular Embryology and Genetics, Kumamoto University, Honjo 2-2-1, Kumamoto 860-0811, Japan.

0012-1606/$ – see front matter © 2009 Elsevier Inc. All rights reserved.
doi:10.1016/j.ydbio.2009.11.013

Interestingly, other reports have shown Cv2 to have an anti-BMP role in various in vitro and in vivo contexts (Ambrosio et al., 2008; Binnerts et al., 2004; Coles et al., 2004; Harada et al., 2008; Kelley et al., 2009; Moser et al., 2003; Rentzsch et al., 2006; Zhang et al., 2007, 2008). For instance, Cv2 exerts both pro- and anti-BMP activities when injected into the zebrafish embryo (Rentzsch et al., 2006). In the *Xenopus* gastrula, Cv2 acts predominantly as an anti-BMP factor (Ambrosio et al., 2008). While endocytic internalization is proposed to contribute to Cv2's anti-BMP activity, this machinery appears to be restricted to a limited range of cell types (Kelley et al., 2009). Biochemical and crystal structure analyses suggest that vertebrate Cv2 may interfere with BMP ligand-receptor binding via its Chordin-type cysteine-rich domain (CR1; Zhang et al., 2007; Zhang et al., 2008), although the in vivo relevance of such molecular interactions remains elusive. More recently, Cv2 was shown to bind other proteins, such as Chordin (Ambrosio et al., 2008), suggesting that Cv2's function is complex, and its role as a pro- or anti-BMP factor may be context-dependent. Therefore, careful investigation is required to identify the in vivo role of Cv2 in different developmental contexts.

Previously, by showing a genetic enhancement between *Bmp4* and *Cv2*, we demonstrated that Cv2 functions as a pro-BMP factor in vertebral and eye development (Ikeya et al., 2006). In the same study, we found kidney defects (hypoplasia) in *Cv2*-null mouse embryos. Our previous report showed that Cv2 acts in the same direction with Kcp, which functions as a pro-BMP factor in a different context (Ikeya et al., 2006; Lin et al., 2005). However, our previous study could not tell whether Cv2 in the developing kidney was required as a pro- or anti-Bmp factor, because of the lack of genetic evidences showing functional interaction between Cv2 and Bmp ligands.

Here, we report that Cv2 plays an essential role as a pro-BMP factor in mouse kidney development. We found that Cv2 promotes the BMP-dependent formation of the cap condensates, and we present genetic evidence that the pro-BMP function of Cv2 is dependent on the presence of Tsg, another BMP modulator. These results demonstrate that an extracellular system for modulating local BMP signals via Cv2 and Tsg plays a key role in the early steps of mouse nephron development.

Materials and methods

Mutant mice and crosses

Mice carrying mutations in *Cv2*, *Bmp7*, *Tsg*, and *Smad1* were described previously (Hayashi et al., 2002; Ikeya et al., 2006; Luo et al., 1995; Nosaka et al., 2003). We crossed $Cv2^{+/-}$ mice with $Bmp7^{+/-}$, $Tsg^{-/-}$ or $Smad1^{+/-}$ mice to obtain compound heterozygotes. No obvious defects were observed in the compound heterozygotes, and we used them for further intercrosses. Genotypes were confirmed by PCR (Ikeya et al., 2006, 2008). Animals were housed in environmentally controlled rooms in accordance with RIKEN guidelines for animal experiments.

LacZ staining, histology, immunohistochemistry, and statistics

LacZ staining, histology, and immunohistochemistry were performed as described previously (Ikeya et al., 2006). Primary antibodies and dilutions were as follows: anti-alpha-catenin, 1:500 (Sigma, rabbit polyclonal); anti-BF2, 1:500 (Abcam, goat polyclonal); anti-cadherin-11, 1:500 (R&D, goat polyclonal); anti-Cv2, 1:1000 (R&D, goat polyclonal); anti-E-cadherin, 1:500 (Takara, ECCD2); anti-β-galactosidase, 1:5000 (Cappel, rabbit polyclonal) or 1:2000 (AbD Serotec, goat polyclonal); anti-laminin, 1:500 (Chemicon, AL-4); anti-NCAM, 1:1000 (Chemicon, rabbit polyclonal); anti-Pax2, 1:200 (Zymed, rabbit polyclonal); anti-phospho-Smad1/5/8, 1:30 (Cell Signaling, rabbit polyclonal); and anti-WT1, 1:50 (Santa Cruz, rabbit polyclonal). For staining with the anti-WT1 antibody, citrate buffer, pH 6, was used for antigen retrieval (Zymed) in a 2100 Retriever (PickCell Laboratories). The anti-Cv2 polyclonal antibody recognizes both N- and C-halves of cleaved Cv2 (data not shown).

The signal intensity of the phospho-Smad1/5/8 staining was compared as follows, using the ImageJ software (National Institutes of Health, Bethesda, MD). We stained sections with phospho-Smad1/5/8-specific antibody and DAPI and acquired images by scanning the sections with a confocal microscope (LSM510 (Zeiss)). The images were trimmed into smaller ones showing either cap condensates or collecting ducts, and we divided the total signal intensity of phospho-Smad1/5/8 in the trimmed regions by DAPI-positive area. We defined this value as the "average signal intensity" of phospho-Smad1/5/8 and compared it across images. No differences were observed among the average signal intensities of the collecting ducts, regardless of the genotype. We regarded average signal intensities from cap condensates that were less than two thirds of the collecting duct average intensity as "reduced."

The numbers of nephrons and nephron progenitors at E18.5 were counted as described previously (Ikeya et al., 2006). We scored eight to 20 embryos of each genotype to obtain these numbers. The number of LacZ-positive cap condensates at E13.5, 14.5, and 15.5 was obtained from six to 30 kidneys from each genotype.

Statistical analyses were performed using GraphPad Prism 4 (GraphPad Software).

Cell culture, transfection, siRNA, and luciferase assay

HEK293T cells were maintained in DMEM/10% FCS (HyClone). To examine the effect of Cv2 on BMP signaling, reverse transfections were performed in a 24-well cell culture plate (BD Falcon) using FuGene6 (Roche, Basel, Switzerland) with a total of 210 ng DNA [100 ng of BRE-luc (Korchynskyi and ten Dijke, 2002), 10 ng of phRL-null (Promega), and the indicated dose of CIG-mCv2 and CIG-LacZ (Megason and McMahon, 2002)] per well, in DMEM/1% FCS. Annealed and purified siRNA duplexes were obtained from Ambion (Austin, TX) and were added at 75 ng per well 4 h prior to the cDNA transfection with X-treme Gene (Roche, Basel, Switzerland). After 16 h of treatment, the cells were lysed and assayed for luciferase activity using the dual luciferase reporter assay system (Promega, Madison, WI), according to the manufacturer's instructions.

Results

Enhancement of hypoplastic phenotypes in the $Cv2^{-/-}$ kidney by $Bmp7^{+/-}$ mutation

We previously demonstrated that *Cv2*-null mice display a reduced kidney size and lower nephron number than wild-type mice (Ikeya et al., 2006). To examine the role of Cv2 during nephrogenesis, we first analyzed Cv2's expression patterns during kidney development in *nLacZ*-knock-in mice ($Cv2^{+/nLacZ}$). At E11.5, the metanephric blastema expressed $Cv2^{nLacZ}$, whereas the ureteric buds were negative for it (Figs. 1A–C). At E12.0, the maturating stromal cells located in the central portion of the kidney became $Cv2^{nLacZ}$-negative (asterisk in Fig. 1D). At E13.5 and E14.5, the $Cv2^{nLacZ}$ expression was mainly restricted to the cap condensates (Figs. 1E–H, and data not shown) and to portions of the forming nephrons (pretubular aggregates, comma-shaped body, and S-shaped body) and Bowman's capsules (Supplementary Figs. S1A–D). Immunohistochemical analyses confirmed that cap condensate cells positive for Pax2 strongly expressed $Cv2^{nLacZ}$, but the peripheral stroma, which was positive for BF2, and collecting ducts did not (Supplementary Figs. S2A–C). From E14 until birth, the $Cv2^{nLacZ}$ expression was restricted to the cap condensates and its derivatives (data not shown).

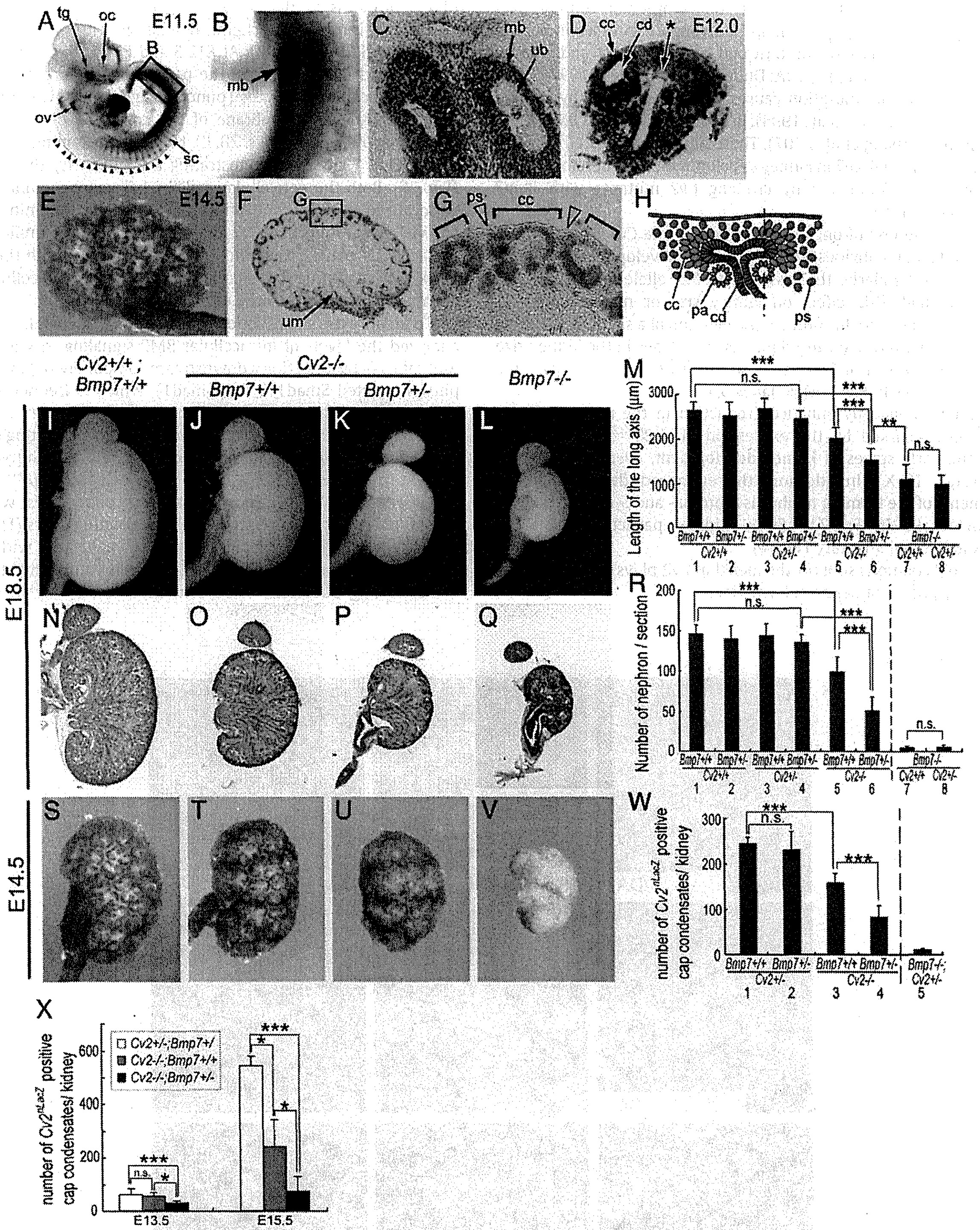

Fig. 1. Cooperative roles of *Cv2* and *Bmp7* in kidney development. (A–G) Expression of *Cv2* analyzed with *nLacZ* knock-in mice. (A–C) At E11.5, LacZ staining was observed in the trigeminal ganglion (tg), optic cup (oc), otic vesicle (ov), sclerotome (sc), roof plate of the neural tube (triangles), and metanephric blastema (mb), but not in the ureteric bud (ub). (D) At E12.0, the central portion of the metanephric mesenchyme became $Cv2^{nLacZ}$ negative (asterisk). cd, collecting duct; cc, cap condensates. (E–G) At E14.5, $Cv2^{nLacZ}$ was preferentially expressed in the cap condensates (bracket in G) and the ureteric mesenchyme (um). Triangles in (G) indicate that the peripheral stroma (ps) was $Cv2^{nLacZ}$-negative. (H) Schematic representation of the cortical region of the embryonic kidney. pa, pretubular aggregate. (I–L) External appearances of the control, $Cv2^{-/-}$, $Bmp7^{+/-}$;$Cv2^{-/-}$, and $Bmp7^{-/-}$ kidneys at E18.5. (M) Length of the long axis. (N–Q) Longitudinal sections stained with hematoxylin and eosin at E18.5. (R) The number of nephrons in the maximal longitudinal sections. (S–V) External views at E14.5 stained with $Cv2^{nLacZ}$. (W, X) The number of $Cv2^{nLacZ}$-positive cap condensates at E14.5 (W, Tukey test), and E13.5 and E15.5 (X, Bonferroni test). Error bars show S.D.; n.s., no significant difference; ***P<0.001; **P<0.01; *P<0.05. In (R) and (W), statistical analyses of the $Bmp7^{-/-}$ samples were performed separately because of significant differences among the S.D.s.

Although these expression patterns, as well as the *Cv2*-null phenotypes, suggest a crucial role for Cv2 in nephrogenesis, the molecular mechanism of Cv2's action, and particularly whether it functioned as a pro-BMP or anti-BMP factor in this developmental context, was unclear. Among the *Bmp* genes, *Bmp7* is strongly expressed in the cap condensate, as well as in the ureteric bud, collecting duct, and forming nephron (Supplementary Fig. S3A; Dudley and Robertson, 1997; Godin et al., 1998), and its mutation causes progressive renal hypoplasia (Dudley et al., 1995; Luo et al., 1995). In addition, Cv2 binds BMP7 with a high affinity (Zhang et al., 2007). These findings suggested that Cv2 might interact with BMP7 in kidney development. We therefore tested their functional interaction by crossing *Cv2* mutants with *Bmp7* mutants (Figs. 1I–X).

At E18.5, the loss of one allele of *Bmp7* in the $Cv2^{+/+}$ or $Cv2^{+/-}$ background had no obvious effects on kidney development (Figs. 1M, R, lanes 1–4). Similarly, the loss of one *Cv2* allele in the $Bmp7^{-/-}$ background had little effect on kidney size or nephron number (Figs. 1M, R, lanes 7, 8). In contrast, the deletion of a single *Bmp7* allele in the $Cv2^{-/-}$ background caused further reductions in the kidney size and nephron number at E18.5 than seen in $Cv2^{-/-}$ mice at the same age (Figs. 1J, K, O, P; Figs. 1M, R, lanes 5, 6).

A similar genetically enhanced reduction in the number of cap condensates (marked by the expression of $Cv2^{nLacZ}$) was evident during the early stages of kidney development, even at E14.5 and E15.5 (Figs. 1S–X). In addition, the enhanced decrease in the components of the forming nephrons (comma- and S-shaped bodies) was obvious in the $Bmp7^{+/-};Cv2^{-/-}$ kidney, particularly at E15.5 (Fig. 1X and Supplementary Fig. S4).

These observations support the idea that Cv2 plays a pro-BMP role in the early phases of nephron formation.

Cv2 is essential for high levels of BMP signaling in cap condensates

These findings prompted us to study the expression and functions of Cv2 proteins in the early embryonic kidney. To this end, we performed immunohistochemical analysis of Cv2 protein in the developing kidney (Fig. 2). At E12.5 and E14.5, the Cv2 protein had accumulated in two regions: the pericellular region of the $Cv2^{nLacZ}$-expressing cap condensates (punctate signals; arrows in Figs. 2G–I) and the basement membrane of the collecting ducts (continuous signals; arrowheads in Figs. 2B, E). No immunostaining was observed in the $Cv2^{-/-}$ kidney, demonstrating the specificity of the antibody (Fig. 2F). Both the pericellular and the basement membrane signals co-localized with fibronectin (Figs. 2G–I) and laminin (data not shown), suggesting that Cv2 protein is densely accumulated in the extracellular matrix. This finding is in accordance with the previous work demonstrating Cv2's co-localization with extracellular matrix (Rentzsch et al., 2006; Serpe et al., 2008).

To identify the site of action of Cv2 in renal development, we next analyzed the levels of intracellular BMP signaling in wild-type and mutant mice by detecting a downstream component of BMP signaling, phosphorylated Smad1/5/8 (pSmad1), which is frequently used to assay BMP activity. At E14.5, high pSmad1 signals were observed in both the cap condensates (cc) and the tips of the collecting ducts (cd) in wild-type and $Bmp7^{+/-}$ embryos (Fig. 3A and Supplementary Fig. S5). In contrast, in $Cv2^{-/-}$, $Bmp7^{+/-};Cv2^{-/-}$, and $Bmp7^{-/-}$ embryos, pSmad1 staining was reduced in the cap condensates, whereas no substantial change was observed in the collecting ducts (Figs. 3B–D). Fig. 3I shows the percentages of cap condensates with reduced pSmad1 signals (in this analysis, signal levels comparable to those in the collecting duct cells were considered to be high). As shown

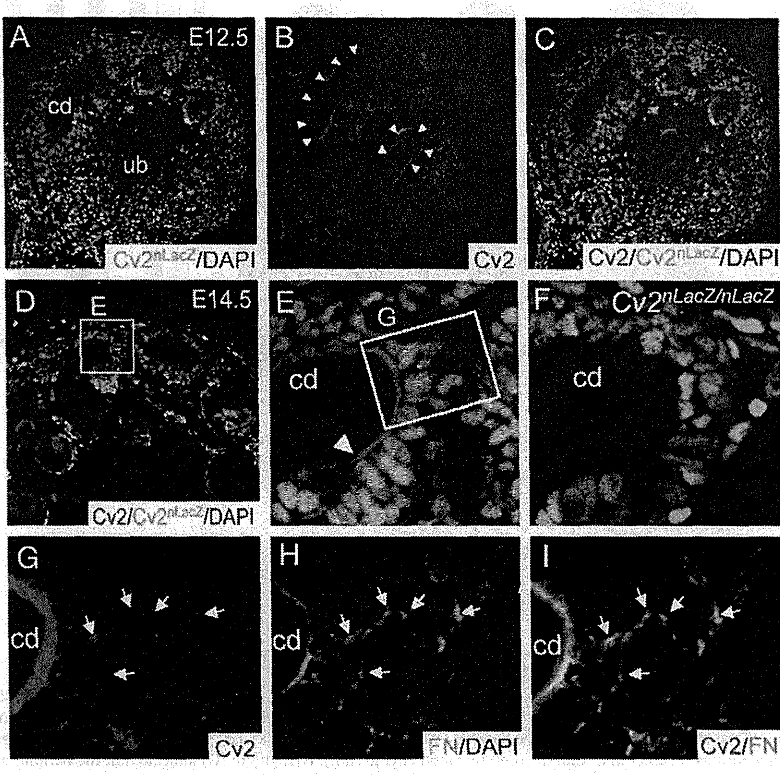

Fig. 2. Distribution of the Cv2 protein. Cv2 protein was accumulated in both the pericellular region of the cap condensate and the basement membrane of the collecting duct. (A–C) Immunohistochemistry with anti-Cv2 antibody at E12.5. Arrowheads, accumulation of Cv2 on the surface of the collecting duct and ureteric bud. (D–I) At E14.5, anti-Cv2 staining was observed in the pericellular region of the $Cv2^{nLacZ}$-positive cells (arrows in G–I) and the basement membrane of the collecting duct (arrowhead in E). (F) No signal was detected in the $Cv2^{-/-}$ mutants. Punctate pericellular signals co-localized with fibronectin (FN; arrows in G–I).

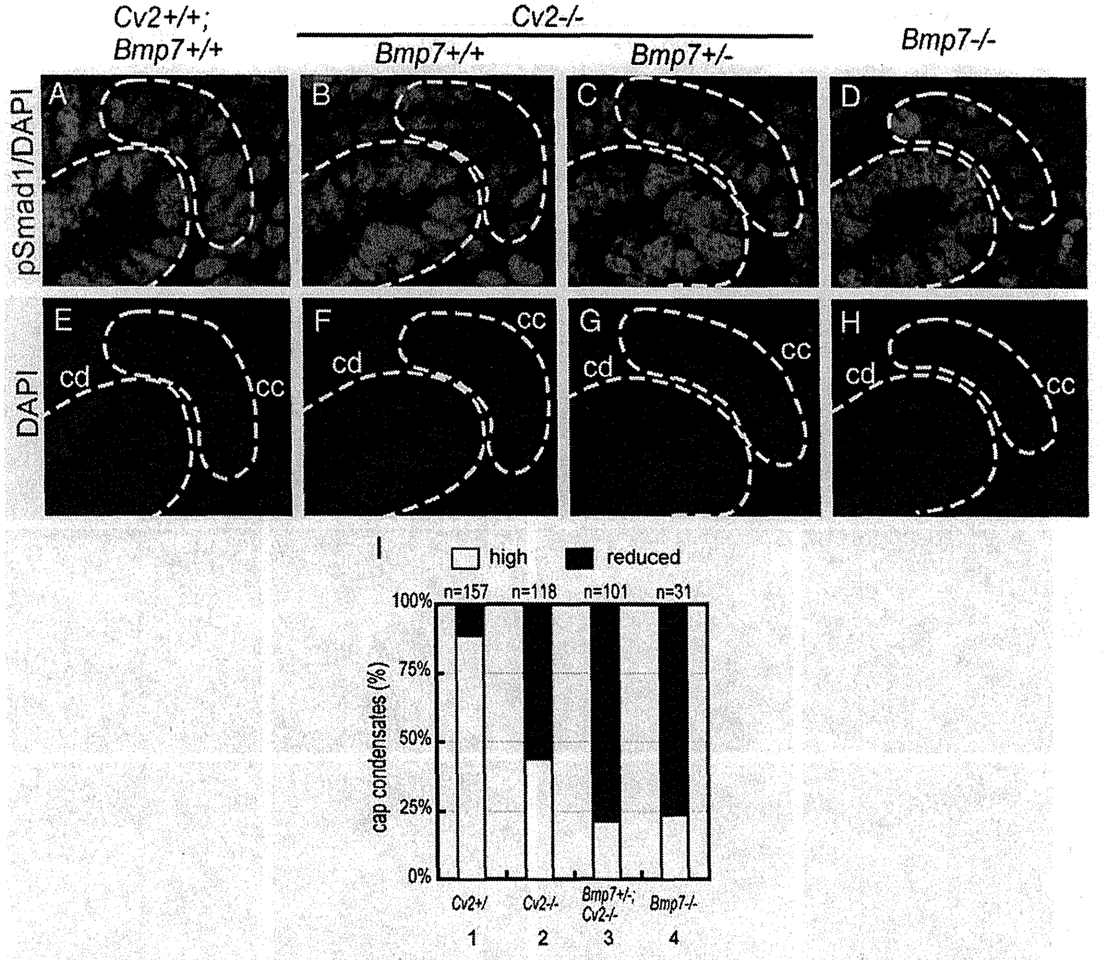

Fig. 3. A pro-BMP role of *Cv2* in the cap condensates but not in the collecting ducts. Staining intensity of pSmad1 was decreased in cap condensates of $Cv2^{-/-}$, $Bmp7^{+/-}$;$Cv2^{-/-}$, and $Bmp7^{-/-}$ kidneys, but it was unchanged in the collecting ducts from all genotypes. Blue, DAPI; red, phospho-Smad1/5/8 (pSmad1)-specific antibody. (I) Percentages of cap condensates showing reduced pSmad1 signal intensity. Under the $Cv2^{-/-}$ background, the $Bmp7^{+/+}$ and $Bmp7^{+/-}$ groups exhibited a significant differences (P value = 0.0007) by Chi-square test.

(Fig. 3I, lanes 2 and 3), the additional deletion of one *Bmp7* allele enhanced the reduction of pSmad1 in the $Cv2^{-/-}$ background, suggesting that Cv2 acts in the same direction as BMP7 (i.e., as a pro-BMP factor).

These observations indicate that Cv2 is essential for enhancing BMP signals in the cap condensate during kidney organogenesis, but that the high BMP signals in the collecting ducts are independent of Cv2, suggesting a tissue-specific mode of Cv2's action.

Incomplete cellular aggregation in the $Cv2^{-/-}$ cap condensates

During nephrogenesis, cap condensates are formed as compact cell aggregates at the tips of the collecting ducts (cc in Fig. 4A). As shown above, BMP signaling was attenuated in the cap condensates of $Cv2^{-/-}$ and $Bmp7^{+/-}$;$Cv2^{-/-}$ mutants. In addition, thin section analysis revealed impaired cell–cell attachment in the $Cv2^{-/-}$ and $Bmp7^{+/-}$; $Cv2^{-/-}$ cap condensates (see loosely packed aggregates in Figs. 4B, C; E14.5), although the cells looked healthy and did not exhibit signs of apoptosis such as picnosis. These observations indicate that the loss of Cv2's pro-BMP function not only reduced the cap condensate number but also caused abnormal cellular aggregation.

Next, we further examined the cellular aggregation by immunostaining. While adhesion molecules such as NCAM and cadherin11 (also alpha-catenin) were distributed uniformly in the cell–cell interface regions in the cap condensate of control embryos (Figs. 4E, I, M), these protein appeared discontinuous or punctate in the $Cv2^{-/-}$ and $Bmp7^{+/-}$;$Cv2^{-/-}$ mutants (arrowheads in Figs. 4F, G, J, K, N, O). These changes did not seem to be caused by a loss of specific cell types, since the cell type-specific markers (Pax2 and p75 for the cap condensate and BF2 for the peripheral stroma) were expressed normally in these mice (Figs. 4Q–S, and data not shown). Rather, these results indicate that a local augmentation of BMP signaling by Cv2 is crucial for the proper formation of cap condensates, including the cap–cell aggregation, during kidney development.

To focus in on which developmental step was most dependent on Cv2, we investigated the marker expression and aggregation of the cap cells in the $Bmp7^{-/-}$ kidney. We found, as reported previously, that the number of $Pax2^{+}$ cells in the $Bmp7^{-/-}$ cap condensates was severely reduced (Fig. 4T; Dudley et al., 1995; Luo et al., 1995). The adhesion molecules were found in a discontinuous pattern (Figs. 4H, L, P), resembling those in the *Cv2* mutants. In addition, the morphology of $Bmp7^{-/-}$ cap condensates were substantially impaired (even more drastically than $Cv2^{-/-}$ and $Bmp7^{+/-}$;$Cv2^{-/-}$ condensates), consisting of cells with a generally round shape (Fig. 4D). These results imply that the complete loss of BMP7 signaling affected the cap condensate in terms of both the cellular presence (Pax2 expression; as reported previously (Dudley et al., 1995; Dudley and Robertson, 1997; Luo et al., 1995)) and the formation of the aggregates. In contrast, the

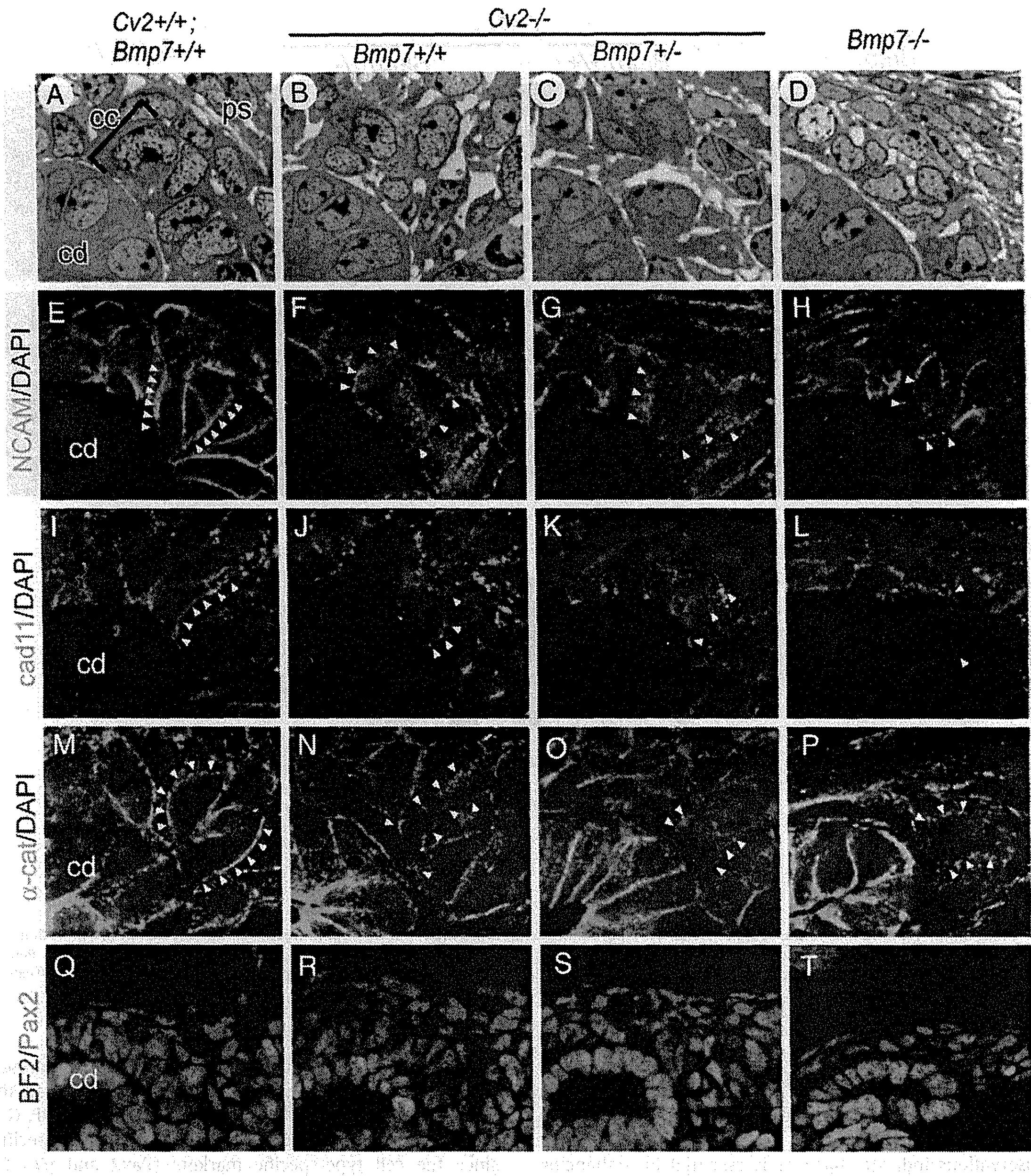

Fig. 4. Cv2 required for the cellular aggregation of the cap condensates. (A–D) Plastic thin sections stained with toluidine blue. In $Cv2^{-/-}$ and $Bmp7^{+/-};Cv2^{-/-}$ kidneys, cap condensate cells adhered loosely to one another. In the $Bmp7^{-/-}$ kidney, the cells on the tip of the collecting duct became round. (E–P) Disturbed distribution of adhesion proteins in the cap condensates of the mutants. Immunohistochemistry with (E–H) anti-NCAM, (I–L) anti-cadherin11, and (M–P) anti-alpha-catenin. (Q–T) Immunohistochemistry with anti-Pax2 (green) and anti-BF2 (red). The Pax2-positive cap condensates and collecting ducts and the BF2-positive peripheral stroma developed normally in the $Cv2^{-/-}$ and $Bmp7^{+/-};Cv2^{-/-}$ mutants. In the $Bmp7^{-/-}$ kidney, the number of Pax2-positive cells was markedly reduced.

attenuation of BMP signaling caused by the loss of Cv2 preferentially impaired the formation of the cellular aggregates.

Tsg mutation is epistatic to the Cv2 mutation in the kidney-defect phenotype

Taken together, our genetic and histochemical analyses demonstrated that Cv2 is an essential pro-BMP factor for the development of cap condensates in the early embryonic kidney. An obvious remaining question is how Cv2 promotes BMP signaling in these cells.

Very recently, two independent studies (from De Robertis' and our groups) reported a genetic interaction between *Cv2* and *Tsg* in skeletal development (Ikeya et al., 2008; Zakin et al., 2008). The major skeletal defects of the *Cv2*-null mutant mice (in the thoracic and lumbar vertebrae) are suppressed in $Tsg^{-/-};Cv2^{-/-}$ embryos, which show moderate skeletal phenotypes (Nosaka et al., 2003; Petryk et al., 2004; Zakin and De Robertis, 2004). This suggests that the *Tsg* mutation is epistatic to the *Cv2* mutation in skeletal development. However, the precise molecular and cellular mechanism of this gene interaction in embryonic development was still unknown.

With this in mind, we examined possible interactions between *Cv2* and *Tsg* in kidney development (*Tsg* expression is detected diffusely in the developing kidney (Supplementary Fig. S3B; Nosaka et al., 2003)). In nephrogenesis, as opposed to skeletal development, interactions with the *Tsg* mutation can be analyzed rather simply, because the *Tsg* mutation itself does not cause significant embryonic kidney

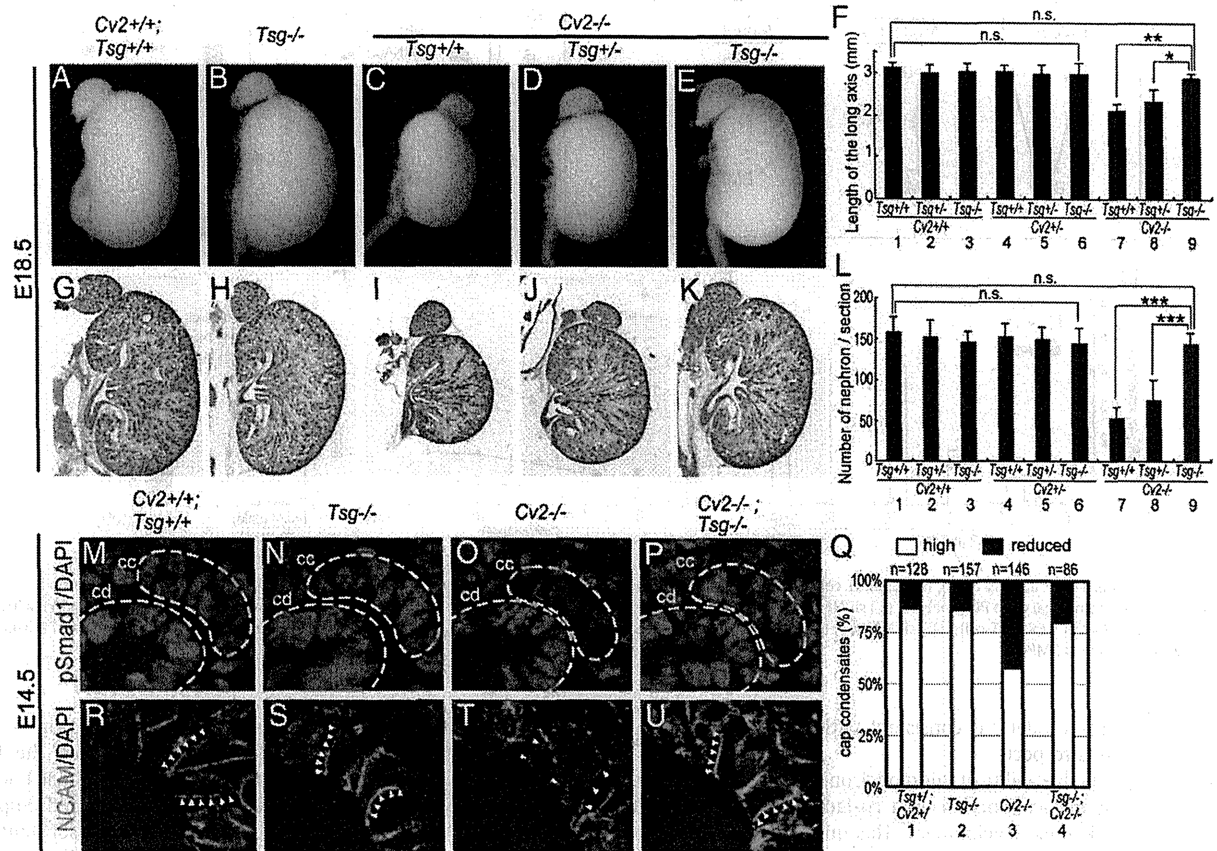

Fig. 5. Evidence for a *Tsg*-dependent pro-BMP function of *Cv2* in vivo. Renal phenotypes of $Cv2^{-/-}$ rescued by the deletion of both alleles of *Tsg* at E18.5 and E14.5. (A–E) External views at E18.5. (F) Length of the long axis. (G–K) Histological sections at E18.5. (L) The number of nephrons in the maximal longitudinal sections. (M–P) Immunohistochemistry with anti-pSmad1 at E14.5. (Q) Percentages of cap condensates exhibiting reduced pSmad1 signal intensity. (R–U) Immunohistochemistry with anti-NCAM at E14.5. Error bars show S.D.; n.s., no significant difference; ***$P<0.001$; **$P<0.01$; *$P<0.05$ (Bonferroni test).

phenotypes (Nosaka et al., 2003). In the $Cv2^{+/+}$ and $Cv2^{+/-}$ backgrounds, the loss of both *Tsg* alleles did not significantly affect kidney size or nephron number at E18.5 (Figs. 5A, B, G, H; Figs. 5F, L, lanes 1–6). In contrast, when combined with the $Cv2^{-/-}$ mutation, the elimination of *Tsg* completely suppressed the renal defects otherwise present in *Cv2*-null mutants (Figs. 5C–E, I–K; Figs. 5F, L, lanes 1, 7–9). The *Tsg* deletion also restored the levels of BMP signaling (reduced pSmad1 levels) in the cap condensates of *Cv2*-null mutants at E14.5 (Figs. 5M–Q) and rescued the impaired cell–cell adhesion in the condensates (Figs. 5R–U).

These in vivo findings suggest a unidirectional dependence in which the pro-BMP function of Tsg requires Cv2, while Cv2 function is not dependent on Tsg activity.

Tsg-dependent mechanism of Cv2's pro-BMP function in cultured embryonic kidney cells

The suppression of the $Cv2^{-/-}$ kidney phenotypes by the *Tsg* mutation implied that, as a whole, Cv2 and Tsg act in opposite directions. That is, they appeared to play pro-BMP and anti-BMP roles, respectively, during nephrogenesis. Interestingly, previous studies suggested that Tsg can act as an anti-BMP or pro-BMP factor, depending on the context (Chang et al., 2001; Harland, 2001; Larrain et al., 2001; Oelgeschlager et al., 2000; Ross et al., 2001; Scott et al., 2001). For instance, genetic interaction studies of mouse *Tsg*-null mutations with *Bmp4* and *Bmp7* mutations show *Tsg* acting as a pro-BMP factor in head development and posterior mesodermal patterning (Zakin and De Robertis, 2004; Zakin et al., 2005). In *Xenopus* embryos, the Chordin–Tsg complex binds to BMPs and inhibits their signaling more efficiently than Chordin, an anti-BMP factor, does alone (anti-BMP activity of Tsg; Oelgeschlager et al., 2000; Scott et al., 2001). In the presence of the Chordin-degrading enzyme Xolloid, on the other hand, Tsg dislodges BMP from cleaved Chordin fragments, resulting in enhanced BMP signaling (a pro-BMP activity; Oelgeschlager et al., 2000).

Given the context-dependent bidirectional functions of Tsg and our findings in this study, the following hypothetical models could explain the functional interaction between Cv2 and Tsg in nephrogenesis. (1) The pro-BMP factor Cv2 and the anti-BMP factor Tsg act independently on BMP signals as simple antagonists (Fig. 6A, Model a). (2) Cv2 acts as a pro-BMP factor by interfering with the anti-BMP function of Tsg (Fig. 6A, Model b). (3) Tsg has simultaneous dual functions as both a pro-BMP and an anti-BMP factor, while Cv2 acts as a co-factor to strengthen the pro-BMP aspect of Tsg's functions (Fig. 6A, Model c).

Given that the fine-tuning of BMP signals is vital for kidney organogenesis (Cain et al., 2008), the phenotypical discrepancy between the normal kidney development of $Tsg^{-/-}$ embryos and the marked hypoplasia of *Cv2*-null embryos is rather difficult to explain with hypothetical Models a and b, which predict hyperactive BMP levels in $Tsg^{-/-}$ kidneys. In contrast, the BMP activity level under the $Tsg^{-/-}$ condition would be less affected in the hypothetical Model c, in which the simultaneous loss of both the anti- and pro-BMP functions could reduce the extent of change in signaling strength (Supplementary Fig. S6B). Consistent with this idea, we have not seen substantial changes in pSmad1 levels in $Tsg^{-/-}$ embryonic kidneys compared with control kidneys (Fig. 5N and our preliminary

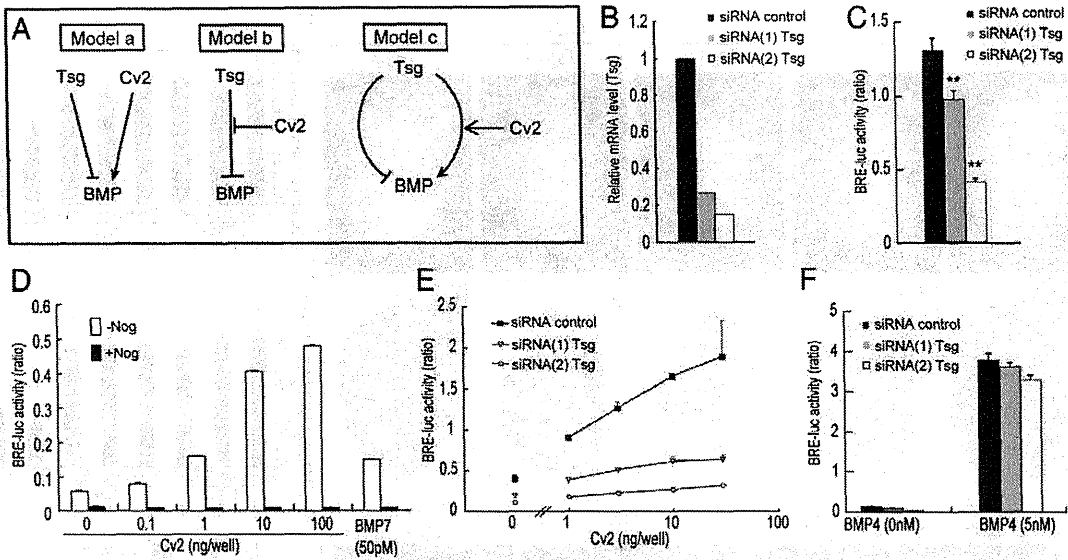

Fig. 6. Cv2 enhances pro-BMP activity of Tsg in HEK293T cell. (A) Models of the interaction between Tsg and Cv2. (B) Knockdown efficiency of Tsg mRNA. Expression levels were determined by quantitative real-time PCR analysis. (C) siRNA targeting of *Tsg* attenuates BMP signaling. Error bars show S.D.; $^{**}P<0.01$ (Dunnet test). (D) Dose-dependent activation of BMP signaling by *Cv2* in HEK293T cells. (E) siRNA targeting of *Tsg* reduces dose-dependent activation of BMP signaling by *Cv2*. (F) *Tsg* knockdown cells respond normally to treatment with high levels BMP4.

observations). Thus, Model c is consistent with the in vivo phenotype, at least in this respect.

To test the predictive ability of this model, one essential question is whether Cv2 can in fact function as a co-factor for the pro-BMP activity of Tsg in kidney development. This question is particularly relevant in light of a *Xenopus* study that suggests that Cv2 enhances the anti-BMP activity of Tsg in a different developmental context (dorsal-ventral patterning during gastrulation) (Ambrosio et al., 2008). Therefore, we next examined whether Cv2 promotes BMP signaling under the condition in which Tsg predominantly exerts a pro-BMP activity over an anti-BMP function.

In a series of preliminary experiments, we found that a human embryonic kidney-derived cell line, HEK293T, expresses *Tsg* as well as *Cv2* and *BMPs* (Supplementary Fig. S7), and that endogenous Tsg acted predominantly as a pro-BMP factor, since, when Tsg was knocked down by siRNAs (see Fig. 6B for the knockdown efficiency), the BMP signaling reporter (*BRE-luc*) activity was reduced accordingly (Fig. 6C). In this cell line, the expression of exogenous *Cv2* (introduced by plasmid transfection) strongly augmented the BMP signal in a dose-dependent manner, showing a pro-BMP activity (Fig. 6D, open columns). This augmentation appeared to depend on extracellular BMP signaling, since the addition of Noggin to the culture medium completely suppressed it (Fig. 6D, closed columns). Importantly, there was little augmentation of BMP signaling by *Cv2* in the *Tsg*-depleted HEK293T cells (Fig. 6E). This absence of the *Cv2*-induced increase in the *Tsg*-depleted cells was not owing to a general loss of the cellular BMP signaling pathway, because the *BRE-luc* activity was strongly stimulated by high concentrations of BMP4 also in these cells (Fig. 6F).

These data show that Cv2 functions as a pro-BMP factor in the presence of Tsg, which has a pro-BMP role in this embryonic kidney cell line, supporting the idea that Cv2 can enhance the pro-BMP activity of Tsg at least under certain situations (Fig. 6A, Model c).

Discussion

In this report, we demonstrated that Cv2 plays an essential pro-BMP role in early nephrogenesis. The cap condensate is the embryonic kidney tissue that normally expresses Cv2, and its development was substantially affected by the *Cv2*-null mutation, even during very early histogenesis. The loss of Cv2 directly attenuated the BMP signaling in this tissue, as assessed by its reduced pSmad1 levels (Fig. 3; in contrast, pSmad2 levels were largely unaffected; Supplementary Fig. S8). In contrast, the *Cv2* mutation did not substantially affect the high BMP signaling levels in the neighboring collecting duct cells, which do not normally express Cv2. Taken together, these observations suggest that Cv2 is a local (or short-range) enhancer of BMP signaling that mainly acts in a tissue-autonomous fashion. In other words, the tissue augments its own BMP response by expressing Cv2.

At least three mechanistic explanations for the context-dependent pro-BMP function of Cv2 have been advocated so far: (1) a cleaved Cv2 protein, rather than a full-length one, exerts a pro-BMP activity (shown in a zebrafish study; Rentzsch et al., 2006). (2) Cv2 is a biphasic BMP modulator acting in a dose-dependent manner that, only at a low dose, facilitates the binding of BMPs to their type I receptor (shown in a *Drosophila* study; Serpe et al., 2008). (3) Cv2 increases the local concentration of diffusible Chordin/Tsg/BMP protein complexes (e.g., on the ventral side in the case of the *Xenopus* embryo), which release active BMPs to their cell surface receptors upon the cleavage of Chordin by tolloid proteinases (proposed in a *Xenopus* study; Ambrosio et al., 2008). In this case, the entrapment of BMP into the complexes is an anti-BMP process, while the release of BMP from the accumulated Chordin/Tsg/BMP complexes (i.e., reservoir complexes for BMP) serves as a pro-BMP step.

Of the three proposals (which are not mutually exclusive), the last one (Mechanism 3) fits our in vivo and in vitro data particularly well. First, our immunostaining results showed that Cv2 proteins are associated with the pericellular matrix (Fig. 2), which could make Cv2 less diffusible. Since Cv2 can physically interact with Chordin, Tsg and BMP (Ambrosio et al., 2008), the Cv2-bound pericellular matrix supposedly contributes to the local accumulation of Chordin/Tsg/BMP complexes. Second, the Cv2-null mutation specifically affected the cap condensates, which are normally surrounded by auto/paracrine Cv2. Third, Cv2 functions as a pro-BMP factor in the presence of Tsg, which is evidence that Cv2 might function in a complex, as proposed for Mechanism 3.